Baseflow Routing and Evaluation in Global River Reaches

by

Abigail R. Baran

A Thesis Submitted in Partial Fulfillment of the Requirements for the Degree of B.A. Honours in Geography

Department of Geography
McGill University
Montréal (Québec) Canada

Acknowledgements

I would like to express my heartfelt gratitude to everyone who has supported and guided me throughout the completion of the honours program and my undergraduate degree.

First and foremost, I would like to express my heartfelt appreciation to my supervisor, Bernhard Lehner, for his invaluable guidance and support throughout this honours thesis. His expertise in handling complex global data, setting reasonable expectations, and fostering self-appreciation for my work has been instrumental in my success. Thank you for your mentorship and encouragement.

I would also like to express my deep appreciation to the Geography Department, for providing me with a stimulating academic environment and access to valuable resources and Michelle Maillet, the undergraduate program advisor, for her encouragement and support.

My sincere thanks go to my family for their unconditional love, support, and encouragement throughout my academic journey and to my friends and honours cohort for their camaraderie, discussions, and feedback that have enriched my research and writing process.

In conclusion, I am grateful to all those who have guided me through my undergraduate program in geography, concluding with this honours thesis. Your support, encouragement, and guidance have been instrumental in the completion of this project. Thank you.

Table of Contents

List of Figures

List of Tables

Abstract

This honours thesis aimed to create a high-resolution map of river reach baseflow indices (BFI) and review graphical baseflow separation methods. Results revealed that BFI is a useful metric for low-flow stability, but caution is needed in equating BFI with groundwater discharge. River reach BFI values are presented in a 15 arc-seconds resolution gridded dataset, developed using flow routing of a course-resolution global BFI from Beck et al. (2015). Validation against gauging stations showed strong agreement (adjusted R2 values of 0.64 and 0.658 for BFI2 and BFI3, respectively) despite uncertainties from source data and baseflow separation. The created BFI maps can be used for global hydrological models, such as temperature or stream chemistry for which baseflow is an important factor; assessing climate change impacts; and sustainability of anthropogenic withdrawals. These presented downscaled and flow-routed maps represent the first estimate of BFI in global river reaches, especially large rivers where graphical baseflow separation methods are not applicable.

Chapter 1 - Introduction

1.1 – Streamflow Definitions

Streamflow or river discharge is the volume of water that passes through a cross-section of a stream channel per unit time, often measured in m^3/s (Fetter, 1988). A hydrograph is a record of discharge over time. Streamflow is derived from multiple sources including direct precipitation into the stream channel; (saturated or infiltration excess) overland flow and shallow subsurface flow, i.e., interflow, caused by a high-intensity rainfall event; snow- or ice-melt; and lakes, wetland, or groundwater discharge. ***Figure 1.1*** conceptually demonstrates the contribution of different sources. Although all sources of streamflow originate from precipitation, the length of time spent in storage before entering the stream and the interactions that the water may have with surrounding rocks or biological actors can alter the temperature and chemistry of water coming from different sources (e.g., Briggs et al., 2018; Reynolds et al., 1986; Peralta-Tapia et al., 2015). These differences both enable the distinction of different sources and demonstrate the significance of separating the contributions from multiple sources to streamflow.

Total river discharge, Q, can be partitioned into multiple components representing the different sources of water in the stream. Water stored in each source has a different residence time, i.e., the amount of time an average molecule of water spends in storage calculated using ***Equation 1.1***, where T_r is the residence time, I is the inflow or outflow into the store, and V is the volume of storage.

$$T_r = \frac{V}{I} \qquad \textbf{1.1}$$

For instance, the residence time of groundwater may be several orders of magnitude greater than water that reaches a stream from saturated overland flow. Hydrograph separation is the process of partitioning the stream discharge and attributing a source to the separated components. Although many flow pathways contribute to river discharge, it is difficult to represent these components as individual curves on the hydrograph and further to specifically identify attribute the source of each curve. Therefore, hydrograph separation commonly refers to the division of discharge into two components.

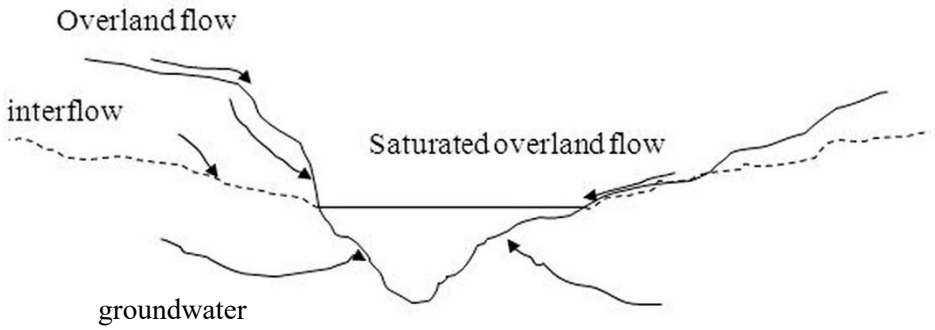

Figure 1.1 *Conceptual diagram of contributions to streamflow from multiple sources. The water table is represented as a dashed line. Saturated overland flow occurs where the water table is at the ground surface. Overland flow on an unsaturated surface occurs when the infiltration capacity of the soil is exceeded by high-intensity rainfall. Inteflow is shallow subsurface flow caused by a storm event, often when a layer with lower permeability is present near the ground surface. Other sources are not illustrated, including lakes, wetlands and snow- and ice-melt (e.g., glaciers).*

The two sources of streamflow considered in hydrograph separation are called, quickflow, Q_s, and baseflow, Q_b. Quickflow, or event flow, is the non-baseflow component of river discharge derived from direct precipitation onto the stream channel, runoff over the land surface, and subsurface stormflow in the uppermost, high-permeability soil layers. Baseflow — sometimes referred to as slow flow, percolation flow, or sustained flow (Hall, 1968) — has varying definitions in the literature. Groundwater discharge and baseflow are often used interchangeably (e.g. Fetter, 1988; van Dijk, 2010). More commonly, baseflow is operationally defined as the low variability portion of the hydrograph through hydrograph separation. According to this definition, baseflow composes groundwater and other delayed sources including, lakes, marshes, snow and ice, stream channel, bank, and temporary depression storage (e.g. Eckhardt, 2005; Bierkens, 2015; Hall, 1968). Although groundwater is thought to be the dominant source of baseflow (Koskelo et al., 2012), in this paper, I will differentiate groundwater discharge and baseflow, such that baseflow is defined as a combination of groundwater discharge and other delayed sources of streamflow. In some settings, it may be appropriate to use baseflow as a proxy for groundwater discharge to streams, if other delayed sources are determined to be negligible (e.g., Miller et al., 2016). The baseflow index (BFI) is defined as the long-term average ratio of baseflow to streamflow. The BFI can be calculated for any period of interest, such as monthly, annually or for the entire duration of the streamflow record, as in this study.

Hydrograph separation can be performed using a physical or chemical characteristic of the water, such as temperature, conductivity, or isotopic signatures, applying multi-component mixing equations. Using even the most advanced techniques, such as $\delta^{18}O$ and $\delta^{2}H$ isotope ratios, uncertainties are still present in assigning the source to each component, as there is often overlap in the isotope ratios from different sources, e.g., similarity in isotope ratios between groundwater-fed wetlands and direct groundwater discharge into the stream (Koskelo et al., 2012). Although the challenges in multi-component mixing increase the uncertainties related to isotopic and chemical hydrograph separation methods, they are still considered superior to baseflow separation methods for accurately determining the contributions from different sources to the stream. However, chemical mass balance methods are difficult to implement and prohibitively expensive at the scale needed for global hydrological studies (Lott & Stewart, 2016; Zekster & Loaiciga, 1993). Therefore, graphical and analytical baseflow separation methods have been developed for use in regional and global scale baseflow studies. Baseflow separation methods are a subset of hydrograph separation methods, as defined here for the purpose of this thesis, and are limited to graphical or analytical analysis of the hydrograph shape. The term hydrograph separation will be used for other forms of baseflow determinations, i.e., separation performed using the stream water characteristics or other catchment characteristics in addition to the hydrograph. In principle, baseflow separation methods assume that quickflow increases faster after a storm event and decreases faster, while baseflow is relatively constant throughout the season, with only minimal, and gradual increases due to a specific event. Longer residence times in groundwater, lake or snow storage, for example, cause attenuation of event peaks: the increase in storage caused by a storm event will be released slowly throughout the coming days, months, or years. Therefore, baseflow separation methods work by identifying peaks in the hydrograph and attributing flashy peaks to quickflow and the stable portion of the hydrograph to baseflow. Chemical hydrograph separation has been used to validate graphical and analytical baseflow separation methods with previous studies finding general agreement (Kissel & Schmalz, 2020; Stewart et al., 2007). Therefore, large-scale studies generally use graphical or analytical baseflow separation methods to separate event-based discharge and stable, low-variability discharge.

1.2 – Significance of Baseflow

The global river network serves as a critical freshwater resource for both aquatic ecosystems and human consumption. The role of baseflow in shaping rivers as viable aquatic ecosystems is noteworthy, as it regulates temperature patterns (Briggs et al., 2018) and the chemical composition of streams (Reynolds et al., 1986; Peralta-Tapia et al., 2015). Compared to quickflow, delayed sources of discharge have more time to equilibrate with their temperature and geochemical surroundings. As a result, baseflow temperature tends to align more closely with seasonal or annual average temperature, while quickflow temperature reflects rainfall/air temperature during precipitation events. Furthermore, baseflow enhances streamflow stability, particularly during dry seasons, due to the longer residence times of baseflow sources. A study conducted by Miller et al. (2016) demonstrated that the Colorado River, which is considered the most overallocated river globally, relies heavily on baseflow to sustain flows during dry periods. Recharge to baseflow sources during rainy seasons can be released gradually throughout the year. The crucial role of baseflow in maintaining streamflow quality and quantity is highlighted by the role of baseflow in controlling temperature patterns and chemical composition of streams, and streamflow stability during dry periods.

1.3 – Vulnerability of Baseflow

The increasing pressures on freshwater resources from human overallocation to unpredictable climatic changes across all scales reinforces the significance of large river systems (Lehner & Grill, 2013). Groundwater and baseflow have specific vulnerabilities to anthropogenic effects and climate change. The groundwater discharge portion of baseflow in a river is sensitive to extraction from the underlying aquifer. Groundwater withdrawals can have unpredictable and non-linear effects on groundwater storage and discharge to streams. Increased anthropogenic discharge from an aquifer via human extraction is accommodated in the water balance by an increase in recharge to the aquifer where possible, a loss in groundwater storage, and/or a decrease in groundwater discharge to streams, contributing to a decrease in baseflow (Theis, 1940). Due to non-linearity, a small change in aquifer storage can cause major changes to surface water sustainability through decreased baseflow (Alley, 2007), especially in semi-arid regions where dry season streamflow is composed primarily of groundwater discharge and/or

snow- and ice-melt. In humid regions, baseflow has been shown to be resilient to groundwater depletion as excess precipitation acts as rejected recharge which replenishes groundwater storage (Khan et al., 2022). The resilience of groundwater discharge to streams derives from the large storage capacity of aquifer systems and associated long residence times (Theis, 1940). In large non-artesian aquifer systems, extraction will at first have a localized effect. After an extended period of ongoing groundwater extraction will the entirety of the aquifer experience depletion causing a reduction in storage or discharge. Therefore, a thorough understanding of the baseflow contribution to the river network allows researchers to identify concerning changes in groundwater storage. A noticeable reduction in baseflow can signify that a large aquifer is affected by groundwater withdrawals. If there is no rejected recharge, this can indicate groundwater depletion. For example, baseflow reductions in the Ganges River have been linked to groundwater depletion (Mukherjee et al., 2018). These complications are likely to increase in the near future as communities look to alternative sources of water, including groundwater. Therefore, it is important to understand the baseflow contribution to global rivers to assess the impact of changing water resource demand through comparisons with the natural state.

Understanding baseflow at the global scale can be used to predict the vulnerability of river systems to climate change and other anthropogenic effects. Climate change can lead to both increases and decreases in baseflow contributions. For example, increased precipitation caused by increasing temperatures in the mid-latitudes and (sub)arctic is expected to increase groundwater discharge to streams in areas without rejected recharge, i.e. groundwater recharge deficits (Zekster & Loaiciga, 1993). Baseflow has also been shown to be sensitive to temperature patterns, either decreasing due to increased evaporation from surface stores and groundwater or increasing due to changes in the meltwater cycle and rainfall/snowfall ratios (Tan et al., 2020). Human-caused land use/land cover changes can also affect the rate and fractionation of water cycle components (Eagleson, 1986). For instance, afforestation has been shown to decrease groundwater recharge and therefore baseflow by increasing summer evapotranspiration and winter evaporation (Alley & Chapman, 2001). Even small changes can affect baseflow, such as a conversion of perennial crops to annual row crops which has been linked to an increase in baseflow in Iowa (Shilling & Libra, 2003). Dams

and infiltration of surface water redirected to irrigation can also increase baseflow by allowing surface water to infiltrate and become groundwater before re-entering streams downstream (Zekster & Loaiciga, 1993). These myriad changes to baseflow can be compared at the global scale in comparison with a baseline of natural baseflow in global rivers.

1.4 – Regional and Global Maps of Baseflow

Maps of the BFI and the recession constant can be made bottom-up from physically based models or top-down from empirical relationships between environmental factors and the two parameters of interest using regionalization. Regionalization describes the process of estimating model parameters in ungauged catchments by correlating known catchment parameters with measurements – or often models – of climate, morphology, hydrogeology, soils, land use, or other environmental variables (van Dijk, 2010). Though both methods have advantages, top-down BFI maps using streamflow characteristics derived from gauged catchment hydrograph data are explored in this study.

There are significant areas on the Earth's surface that are ungauged or poorly gauged (Fekete & Vörösmarty, 2002). Regionalization enables investigators to use knowledge of gauged basins to understand hydrological processes in ungauged regions. The choice of climatic and physiographic variables and the baseflow separation or recession constant determination method affect the resulting maps of BFI and k. Baseflow has been previously mapped in various regions across the globe, with particular attention to areas where surface water resources are overallocated, such as the Upper Colorado River Basin (Miller et al., 2016), the state of Texas (Aboelnour et al., 2021), and southern Italy (Longobardi & Villani, 2008). Regionalized BFI and k also exist for large regions. For instance, BFI regionalization has been performed for continental Europe (Schneider et al., 2007), the contiguous United States (Santhi et al., 2008; Neff et al., 2005; Wolock, 2008), and Australia (Van Dijk, 2010). Pena-Arancibia et al. (2010) produced a map of k across the tropics.

Beck et al. (2013, 2015) performed the first global-scale regionalization of BFI and the recession constant through regionalization. They first calculated BFI for over 3,000 gauging stations using graphical and analytical baseflow separation methods. They then employed regionalization to relate catchment-specific BFI values and various

climatic and physiographic features to create the global maps. The gridded BFI and *k* maps are at 0.125° x 0.125° resolution (each cell represents about 190 km² at the equator). The Beck et al. (2015) maps represent the local baseflow contribution from each cell (see *section 3.1* for more information). Beck et al. (2013) suggest further validation of the global BFI and k maps is needed.

1.5 – Applications of Global Baseflow Maps

Beck et al. (2013) envisioned applications of their work in the diagnosis and parameterization of land surface schemes, global hydrological models, water resource assessments, and catchment classifications. Baseflow can be used as an input layer to global-scale hydrologic models, which have a wide variety of applications including studies on food systems, energy resources, biodiversity assessments, and hydro-climatology (Bierkens, 2015). Baseflow models are also used to forecast low flows that occur during the growing season (Hall, 1968). These models can incorporate aspects of the complex coupled human-natural system to respond to future changes, where baseflow serves as a fundamental link between surface water and groundwater (Miller et al., 2016). Baseflow can also serve as input data for modelling watershed export of materials of interest that may be derived from groundwater or lakes and marshes, for example, sediment, contaminants, or geochemical compounds derived from aquifer solids (Koskelo et al., 2012).

Global hydrology is needed because there are significant contributions to water cycle elements which are connected to processing occurring outside of the catchment in most climates (Eagleson, 1986), such as forest evapotranspiration driving distant precipitation (Ellison et al., 2017). Global hydrological models facilitate water management decisions, especially where free and high-resolution global-scale datasets are available. Early global hydrologic models did not account for baseflow, instead using rudimentary modelling of runoff processes without accounting for local geology and shallow subsurface interactions (Bierkens, 2015). It is necessary to account for the groundwater contribution to global water circulation to complete global water balance calculations (Zekster & Loaiciga, 1993).

Baseflow determinations on a global scale are significant because they facilitate international water resource management and comparisons between different regions.

Most large aquifers span multiple jurisdictions and require transboundary efforts to manage sustainably (Richts et al., 2011). Global studies can account for these scenarios, where regional studies are often limited by political boundaries. Comparisons between regions can be uniquely facilitated by global studies, owing to the continuity of data quality and resolution. Beck et al. (2013) compared their global maps with a subset of previous regional studies as validation. They found general compatibility between the maps and attributed small differences to the choice of baseflow separation method. For this reason, a global map represents a significant step forward as these small systematic differences between regions are not compatible with global-scale comparisons. In this sense, it would be impossible to confidently attribute changes to actual stream conditions between regions. The differences between the maps could also derive from other factors, including the regionalization data and processes and the gauging station data quality and availability.

1.6 – Flow Routing

The existing global-scale and regional BFI maps are limited in their applicability to relatively small river systems and catchments, typically with upstream areas of less than 10,000 km^2, due to the constraints of graphical baseflow separation methods (as discussed in ***Chapter 2***). Beck et al. (2013) suggest that the effects of river channel routing should be accounted for when using the maps for larger catchments. According to Lehner and Grill (2013), "routing refers to the simulation of transport processes over space and time". Flow routing simulates the generation of streamflow from runoff, or the downstream movement of water in streams, by modelling the inflow and outflow from surface and sub-surface reservoirs using a land surface parameterization that is typically built upon a digital elevation model (DEMs) (Arora et al., 2001; Lehner & Grill, 2013). There are two primary methods of flow routing: hydrodynamic routing, and hydrological routing. Hydrodynamic routing applies the Saint-Venant equations which describe the balance between input, storage, and output in a river using momentum equations (Arora et al., 2001). Hydrological routing methods rely on a simplified conceptual approach where water is modelled as accumulating downstream, i.e., water is passed to the next downstream storage 'bucket' (Weinmann & Laurenson, 1979).

Hydrological routing is often preferred because the former method is more complex and requires data that are difficult to obtain.

In this study, I will use hydrological flow routing to determine the BFI along the river network, in every river reach. A river reach, according to a cartographic definition, is the river segment between two neighbouring confluences. Beck et al.'s (2015) BFI maps represent the local contribution of each cell to downstream BFI. Using hydrological routing, I will calculate the BFI of streamflow passing through each cell, considering the upstream and local contributions to baseflow. This map will serve as a first estimate the BFI in global river reaches and the first estimate of baseflow in rivers that are too large for the application of baseflow separation methods.

Flow routing using high-resolution input data and the coarse-resolution BFI maps from Beck et al. (2015) will facilitate downscaling of the BFI maps to 15 arc-second x 15 arc-second resolution. At the equator, a 15 arc-second square cell is approximately 0.2 km^2, the same area as Grand Central Station in NYC. The cell areas decrease away from the equator. This downscaling will serve as additional validation for the Beck et al. (2015) BFI maps. Most global scale hydrological data and models are available as low-resolution gridded datasets, where each cell represents the average of each characteristic for the land surface that it represents. These models have been criticized for obscuring connectivity features, especially for use in aquatic ecosystem applications (Lehner & Grill, 2013). The downscaled BFI maps will be the first high-resolution, global maps of baseflow in rivers. The high-resolution format also allows the data to be usable at local or regional scales. The BFI maps emphasize hydrological connectivity due to the continuity of baseflow estimates along rivers, allowing the baseflow patterns to be examined along a river.

1.7 - Objectives

The overarching goal of this thesis is to determine the baseflow index of every river reach globally. To achieve this goal, it is divided into 3 supporting objectives: (1) evaluate the theoretical foundations of baseflow separation, (2) downscale the coarse-resolution BFI maps from Beck et al. (2015) to create a high-resolution global map of BFI considering the upstream and local contribution to baseflow in each cell, and (3)

validate the high-resolution BFI map against BFI values calculated at almost 3,000 gauging stations using graphical baseflow separation.

Chapter 2 – Review of Baseflow Separation

Many baseflow separation methods have been developed in the past 150 years to determine the baseflow component of streamflow. Baseflow separation may be better described as an art than a science given the significant uncertainties in the process from the definition of baseflow itself to the underlying assumptions (Bedient et al., 2013). Baseflow separation is a theoretical or operational separation of quick and slow contributions to streamflow, i.e., quickflow and baseflow, respectively. Baseflow separation is theoretical as the hydrograph does not inherently contain differentiations of the components (van Dijk, 2010). Rather, the separation is determined by analyzing the shape of the hydrograph. Regional baseflow studies and Beck et al. (2013, 2015), using a variety of baseflow separation methods, have found statistically significant relationships between BFI and catchment characteristics which suggests that the baseflow determination is at least linked to climatic and physiographic conditions, confirming that graphical and analytical baseflow separation methods capture at least some representative low-flow and stable-flow features of streams across large scales.

2.1 – Boussinesq and Barnes Baseflow Equations

The Boussinesq equation (***Equation 2.1***) was first proposed by Joseph Boussinesq in 1903 and again, independently, by Edmond Théodore Maillet in 1905 (McMahon & Nathan, 2021) to mathematically explain the discharge of a large unconfined aquifer to a stream when there is no evapotranspiration, leakage to deeper groundwater, nor recharge (Tallaksen, 1995). In ***Equation 2.1***, $Q(t)$ is the discharge at time t, often measured in days; $Q(0)$ is the discharge at the peak; and α is the recession rate. Many subsequent methods are based on the Boussinesq equation and rely on the same set of assumptions (see McMahon & Nathan, 2021, for a thorough review of Boussinesq-based baseflow separation methods).

$$Q(t) = Q(0)e^{-\alpha t} \qquad \textbf{2.1}$$

$$Q(t) = -kS(t) \qquad \textbf{2.2}$$

where

$$k = Ce^{-\alpha t} \qquad \textbf{2.3}$$

An alternative form of the Boussinesq equation (***Equation 2.2***), defines k as the recession constant in ***Equation 2.3*** (Barnes, 1939), and S as the reservoir storage,

based on the assumption that aquifer discharge is linearly proportional to its storage and decreases exponentially during baseflow recession, and C is an arbitrary constant. This form implies the following relationship between baseflow on a given day during the hydrograph recession period, a period where there is no rainfall or recharge to baseflow source stores (***Equation 2.3***).

$$Q(t) = Q(t-1)e^{-k} \qquad \textbf{2.4}$$

The Boussinesq equation is a linear approximation to the solution of the non-linear differential equation which governs the unsteady flow from an idealized aquifer (Vogel & Kroll, 1996). Although groundwater discharge and the contribution from other delayed sources are non-linear, investigators commonly approximate baseflow processes as linear (McMahon & Nathan, 2021). Van Dijk (2010) showed that the baseflow estimates produced from a linear reservoir model were commensurate with a non-linear model, suggesting that linear approximation is an appropriate simplification for baseflow processes.

It is outside the scope of this study to provide a review of all available baseflow separation methods. Thorough reviews of methods are provided by McMahon & Nathan (2021), Nathan & McMahon (1990), and Tallaksen (1995). Eckhardt (2005, 2008) provides a review of recursive digital filtering methods, a type of hydrograph-based analytical method. Recently, more complex graphical and analytical baseflow separation methods have become available. For instance, Koskelo et al. (2022) developed a coupled precipitation-streamflow method and Wang et al. (2023) combined a recursive digital filtering method with an analysis of the flow duration curve to separate the sources of baseflow in discontinuous permafrost regions. These special-purpose methods integrate external parameters and are designed to work in specific situations where data are available, such as very small catchments (<50 km^2) for the former method.

2.2 – Baseflow Separation Methods for Global Studies

Many baseflow separation methods are not appropriate for application on a global scale for a variety of reasons. Beck et al. (2015) selected four baseflow separation methods to develop their global BFI maps. I have identified the following criteria that enable their methods to be applicable on a global scale. Beck et al. (2013, 2015) do not provide a justification for their choice of methods or any evaluation of the assumptions and

limitations of their selection. The methods must be automated, such that they can be applied easily for thousands of hydrographs each containing more than 10 years of daily data. The chosen methods must work well for all global climates for which there is gauge data. For example, methods must be suitable for hydrographs with zero flow days (or weeks, or months). The methods also must provide sufficient differentiation between regions to allow for regionalization. Beck et al. (2015) further limited their method selection to those that work with Q in mm/day and do not require additional data beyond daily streamflow, such as precipitation or soil parameterizations. The four methods that they selected are presented in ***Table 2.1***. ***Figure 3.2*** shows an example of baseflow separation using all four methods. Although only one of the four baseflow separation methods used by Beck et al. (2015) is directly derived from the Boussinesq equation, ***Equation 2.3*** provides the theoretical foundation for most graphical and analytical separation methods including all selected methods used by Beck et al. (2015). Therefore, the underlying assumption of the four methods are explained in the previous section.

Table 2.1 *Baseflow separation methods used to develop local BFI maps by Beck et al., 2015. The methods are described in detail in Chapter 3 – Methods.*

	Method	**Parameters**	**Source**
1	Recursive Digital Filtering	window = 5 days	Van Dijk, 2010
2	Local-Minimum (HYSEP)	duration of surface runoff (N) = 5 days window = 11 days	Pettyjohn and Henning, 1979; Sloto and Crouse, 1996
3	Sliding-Interval (HYSEP)	duration of surface runoff (N) = 3 or 4 days window = 7 days	Pettyjohn and Henning, 1979; Sloto and Crouse, 1996
4	Non-Overlapping Interval Local-Minimum	window = 5 days	Gustard et al., 1992

2.3 –Recession Constant

Many baseflow separation methods require at least one parameter, typically the baseflow recession constant, k. A recession period of a hydrograph represents the period of discharge decline after a storm event, while there is no additional precipitation or recharge of stores. While the hydrograph recession period is simply the length of time between recorded storm events, i.e., discharge peaks, quickflow and baseflow recession are determined by the properties of the catchment. Quickflow and baseflow recession periods are defined as the length of time between the event peak and the return to the

pre-event flow rate. Residence times are inversely related to the recession rates for quickflow and baseflow (Tallaksen, 1995). Quickflow peaks shortly after the storm event and diminishes rapidly from the peak in the following hours, days or weeks, depending on the size of the catchment and other climatic and physiographic factors (Fetter, 1988). Baseflow recession occurs more slowly than quickflow recession, indicating that the baseflow recession period is longer than the quickflow recession period. The hydrograph recession period may also be longer than the quickflow recession period. If this is the case, then the hydrograph will record a period where streamflow is entirely composed of baseflow. The recession constant is a measure of the baseflow recession rate (***Equation 2.3***)

Although Beck et al.'s (2013) map of the recession constant is not used in this thesis, the recession constant is a parameter for baseflow separation method 1. Therefore, the baseflow in river reaches using BFI1 is reliant on the recession constant as calculated by Beck et al. (2013, 2015) using ***Equation 2.4*** during periods identified as a hydrograph recession for each gauge station following van Dijk (2010). Although the recession constant is often considered only in the context of baseflow defined as groundwater discharge, all delayed sources of streamflow should experience recession behaviour during the period of no recharge as precipitation slowly moves through the systems toward an outlet. Each baseflow source will have a different recession constant. The *k* value determined by the following procedure can be thought of as a weighted average of the recession constant for each component of baseflow.

Equation 2.4 relies on the assumption that after a period of *T* days from a storm event, quickflow does not measurably contribute to discharge, i.e., *T* is the length of the quickflow recession period. Van Dijk (2010) used *T*=10 days, while Beck et al. (2013) used *T*=5 days. From day *T+1* until the end of the hydrograph recession period, data pairs of Q and Q^* were fit to ***Equation 2.5*** to determine k. The end of the hydrograph recession period is marked by an increase in Q from one day to the next.

$$k = -\ln\left(\frac{Q}{Q^*}\right) \qquad \textbf{2.5}$$

where

$$Q = \exp\left(\overline{\ln\left(Q(t = 1,2,3, \ldots)\right)}\right)$$

$$Q^* = \exp\left(\overline{\ln\left(Q(t = 0,1,2, \ldots)\right)}\right)$$

The choice of *T* must balance the effect of remaining quickflow on the recession and the availability of long hydrograph recession periods in the hydrographs (van Dijk, 2010). The number of hydrograph recession periods of at least a given length decreases quickly as the length increases. The recession constant derived from hydrographs is highly related to the length of the hydrograph recession period analyzed (Vogel & Kroll, 1996). Analyzing individual hydrograph recession periods results in baseflow recession constants that vary by as much as 35% (Halford & Mayer, 2000). The choice of a small *T* maximizes the number of hydrograph recession periods that are analyzed. Errors in *k* estimation are thought to derive primarily from the finite and often short duration of hydrograph recession periods from a given hydrograph (Vogel & Kroll, 1996). This effect may be enhanced by the shorter *T* used in Beck et al. (2013, 2015) in comparison to other studies, as the recession lengths are biased toward short hydrograph recession periods.

Any choice of *T* assumes that quickflow decreases to zero in a finite period of length *T*, which has not been verified (Halford & Mayer, 2000; McMahon & Nathon, 2021). If this is the case, a selection of a shorter *T* for a global recession constant determination may increase the calculated recession rates if the true quickflow recession takes more than *T* days. The quickflow recession period, *T*, may also vary greatly across the globe or throughout the year. In addition, some investigators have predicted that the baseflow recession rate is generally faster in the summer than in the winter due to differences in evapotranspiration (Tallaksen, 1995), although this effect may be more pronounced in catchments with shallow water tables and abundant deeply rooting vegetation (Eckhardt, 2008). The confounding effects of these influences lead to significant uncertainty in the recession constant. Beck et al. (2015) found the greatest variability in the *k* map compared to all other streamflow characteristics that they calculated. They also found the weakest correlation between *k* and the climatic and physiographic catchment characteristics. Therefore, BFI1, whose separation method relies on the recession constant assumes greater uncertainty due to the complications in determining *k*.

Chapter 3 – Methods

3.1 – Local BFI Data

Beck et al. performed the first global-scale regionalization of the baseflow index (BFI) and the recession constant in 2013 using data from 3,394 gauging stations located across the globe. BFI is defined as the long-term average baseflow to streamflow ratio and is represented as a number between 0 and 1, although the regionalization process used by Beck et al. (2015) results in some cells with extraneously high or low values. In 2015, they produced three additional maps of BFI using different baseflow separation methods. Both studies define baseflow as the contribution of delayed sources to streamflow, i.e., including contributions from lakes, wetlands, or snow storage. Their global gridded maps are provided at 0.125° x 0.125° grid cell resolution. The regionalization was performed using various climatic and physiographic catchment characteristics which were associated with streamflow data using catchment boundaries produced by Lehner (2012). These characteristics were associated with BFI and *k* using an Artificial Neural Network and ten-fold (twenty-fold in Beck et al., 2015) cross-validation of a random subset of the gauge stations to train and validate the model. An independent set of stations was used to determine the significance of the inputs for each of the model runs. The most significant predictors of BFI were the aridity index, precipitation, surface slope, snow cover, and topographic wetness index. The least significant of the investigated predictors were those related to geology and soils. Of this group, the percentage of clay had the greatest predictive power. Beck et al. (2015) note that although geology is known to affect baseflow, the data quality may limit the use of subsurface data for global-scale studies. The maximum catchment size considered was 10,000 km^2 (5,000 km^2 in the most recent version available and used in this thesis to downscale BFI). They suggest that larger catchments may have inflated BFI due to channel routing effects and that the maps should not be used to understand BFI in larger rivers due to these effects. In this study, the global BFI maps from Beck et al. (2013, 2015) will be referred to as local BFI maps as the BFI for each cell represents the fraction of water derived from that cell that eventually reaches a stream as baseflow. The data are available at http://www.gloh2o.org/gscd/.

3.2 – Global Underpinning Hydrography Data

Global underpinning hydrography data was sourced from HydroSHEDSv1, a collection of consistent and comprehensive gridded hydrological datasets developed to support regional and global watershed analyses, hydrological modelling, and freshwater conservation planning (Lehner et al., 2008). The core data layer of HydroSHEDSv1 is a conditioned digital elevation model derived from the Shuttle Radar Topography Mission (SRTM) (Farr & Kobrick, 2000) at a cell resolution of 3 arc-seconds and subsequently upscaled to resolutions of 15 and 30 arc-seconds (Lehner et al., 2008). More information on HydroSHEDS is provided at http://www.hydrosheds.org. In this study, I used the flow direction map with a resolution of 15 arc-seconds. This gridded dataset contains the most likely direction of flow from a cell to one of its eight neighbours. This layer is used for flow accumulation.

Gridded runoff data was sourced from HydroATLAS, a database containing a uniform compilation of detailed hydro-environmental data for global catchments, presented at high spatial resolution (15 arc-seconds), including a sub-database of world rivers called RiverATLAS. HydroATLAS is part of the HydroSHEDS suite. Runoff data are based on long-term (1971–2000) average 'naturalized' discharge and runoff values provided by the globally integrated water balance model WaterGAP (Döll et al., 2003). The WaterGAP data were spatially downscaled from their original 0.5° cell resolution (~50 km at the equator) to the 15 arc-second (~500 m) resolution of the HydroSHEDS river network using geo-statistical techniques (Lehner & Grill, 2013). Gridded cell area data was also sourced from HydroATLAS and represents the area of each 15 arc-second cell in km^2.

3.3 – Gauging Station Data and Preparation

Daily streamflow data used for validation of the BFI flow routing maps were sourced from the World Meteorological Organization Global Runoff Data Centre (GRDC) database. This database contains approximately 10,000 gauging stations of various data consistencies and record lengths. Each streamflow record had been previously quality checked through statistical and manual outlier detection and primarily regulated streamflow stations were excluded (see Messager et al., 2021). Each station had also

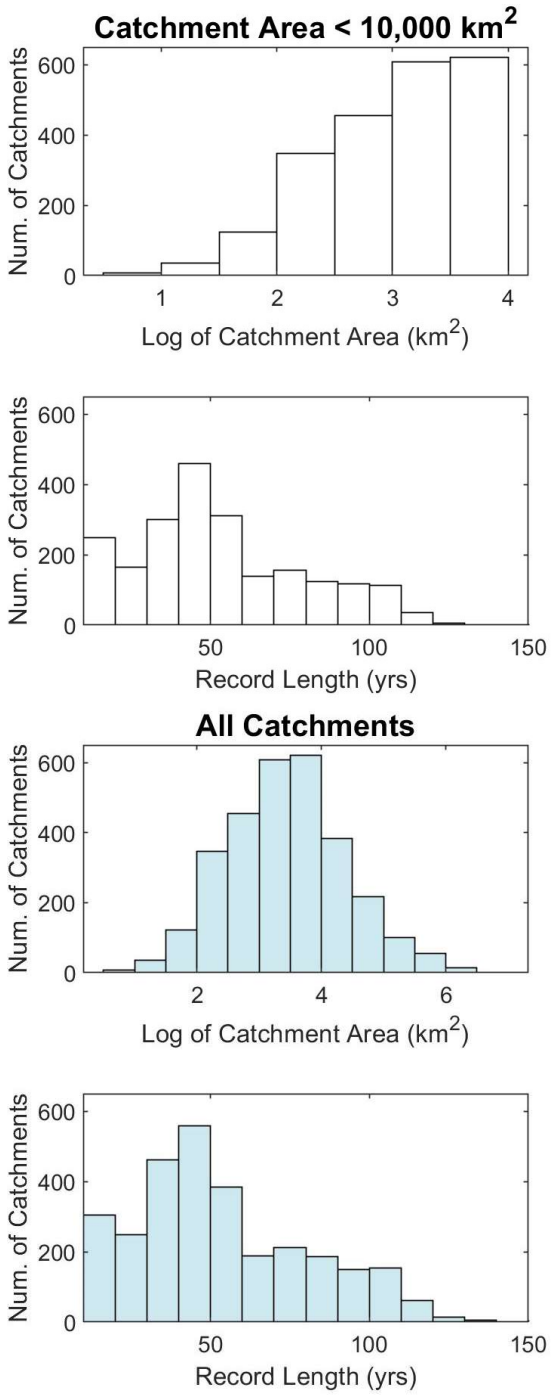

Figure 3.1 *Histograms of Catchment Size and Record Length. The top graphs in white are limited to catchments smaller than 10,000 km². While the bottom two figures in blue show all catchments. The Record Length indicates the entire period over which streamflow is available for a station, rather than the continuous period of data availability.*

been geographically linked with a river reach in the RiverATLAS stream network. RiverATLAS contains a vector representation of every river reach including stream characteristics (Linke et al., 2019). The pre-filtered and geographically linked set of 6,722 gauging stations was used for this project.

The GRDC data is provided in text file format including catchment data, such as the latitude and longitude, station altitude, and the range of dates provided. Daily data is provided in four columns, the date, original and calculated streamflow, and a flag column indicating whether the streamflow was corrected. The flag is rarely used, so I chose to ignore this column. I loaded the data from text file format into python as a dictionary of dataframes containing the daily streamflow data for each station (see *Supplementary Materials* for code, *S1: Get Filenames Function*, *S2: Load Data Function*). I then calculated the length of continuous data for each station. I limited the station selection to stations with continuous data for 10 years or more containing gaps no longer than five days with fewer than 10% missing data. I separated each continuous period for each station into a separate dataframe. By considering separate continuous periods from a single gauging station – each gauging station record may be composed of multiple periods of 10 or more

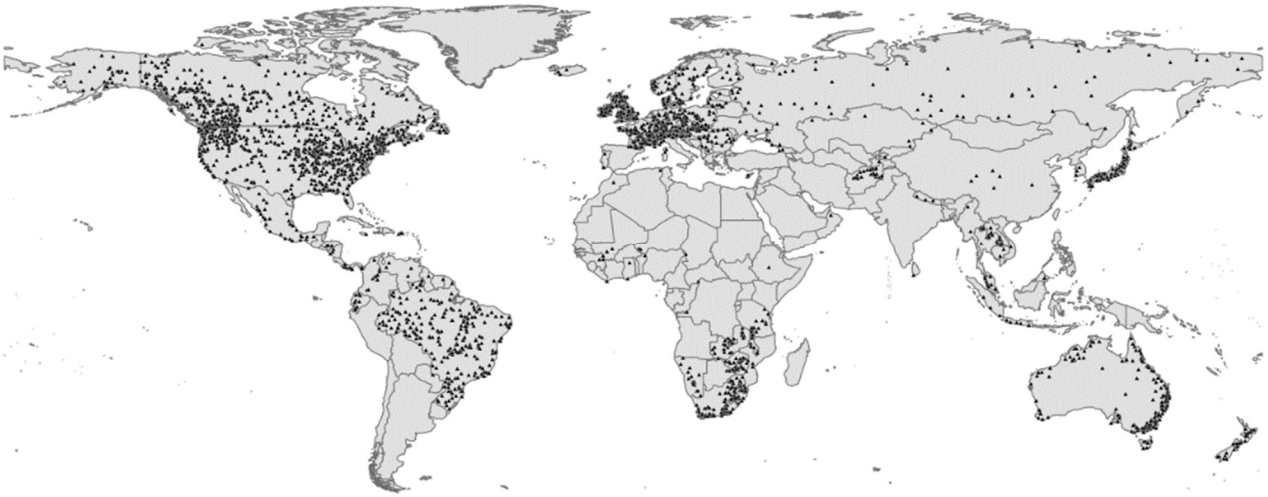

Figure 3.2 *Map of Selected Gauging Stations. Stations are represented as black circles; country borders are outlined in black. Stations are concentrated in North America, Europe and select countries (Brazil, South Africa, Australia, New Zealand, and Japan). Gauging stations cover a wide range of climate types. There are very few catchments located in the Arctic.*

years of consecutive data – I ensured that as much usable data was kept as possible to reduce the bias in the data selection. A 10-year recording period may not account for changes in streamflow behaviour over time nor interannual variability. However, a longer threshold would eliminate much of the available data. The period of five missing days was chosen as the selected baseflow separation methods are tolerant to missing periods of five or fewer days. To simplify the BFI calculations, the data gaps were filled by linearly connecting the recorded data on either side of the gap (*S3: Fill Gaps Function*). The calculated BFI for the station is reported as the total baseflow divided by the total streamflow calculated continuously across the entire set of station data. This method allows stations with temporally heterogeneous reliability to be included if any period of sufficient length within the entire record meets the criteria. After selection criteria were applied, 2,941 stations were remaining.

The selected gauging stations are mainly located in the Americas, Europe, and Australia (***Figure 3.2***). The upstream area represented by each gauging station was previously calculated by using flow accumulation weighted with the HydroATLAS cell area and extracting the upstream area at the gauging station locations. Approximately 75% of gauge stations had an upstream area of less than 10,000 km^2, and 62% had an upstream area of less than 5,000 km^2 (***Figure 3.1***).

3.4 –Station BFI

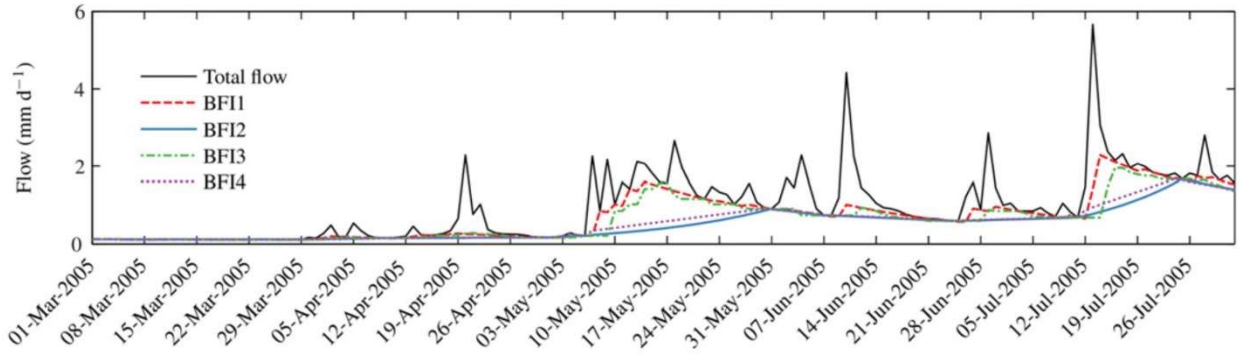

Figure 3.3 *Time Series of Recorded Discharge from USGS Catchment 50145395 (Rio Casei above Hacienda Casei, Puerto Rico; catchment area is 19 km²) and Computed BFI1-4 (from Beck et al., 2015).*

I calculated the BFI for 2,941 daily streamflow records using the baseflow separation methods selected by Beck et al. (2015). The descriptions of the four baseflow separation methods are presented below. An example of baseflow separation using each of the four methods is presented in ***Figure 3.3*** from Beck et al. (2015).

BFI1. The first baseflow separation method is a recursive digital filtering method adapted from the Boussinesq equation by van Dijk (2010). First, the recession constant is calculated using ***Equation 2.5***. Then BFI1 is calculated by applying ***Equation 2.4*** to the streamflow time series both backwards and forwards. The backwards run considers *Q(t)*, and *Q(t+1)* rather than *Q(t-1)*, and *Q(t)* as in the forward run. Then, the decision tree presented in ***Figure 3.4*** is used to assign either the backward or forward baseflow estimate. This algorithm effectively creates a window of length of 3 days. Baseflow increases on the second day of a streamflow peak then decays until the next storm event. The magnitude of the baseflow peak following a storm event is dictated by *Q* recorded on the second day of the streamflow peak and the rate of decay is governed by the recession constant (see *section 2.3*). The baseflow curve derived using this

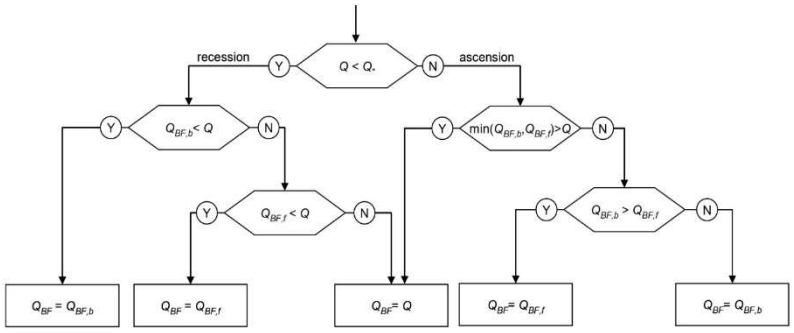

Figure 3.4 *Decision Tree used in BFI1 Calculation (from van Dijk, 2010). The selection of a baseflow value for each day in the time series is calculated using* ***Equation 2.4****, then determining whether the day has more or less streamflow than the previous day.*

method closely follows the hydrograph curve during the recession period, as it is assumed that the quickflow recession period lasts 5 days (T = 5 days, see *section 2.3*). The recession constant is a highly uncertain value for record lengths shorter than 30 years as there are too few long recession periods to constrain the fitted value. This reduces the streamflow records available for validation. This method also predicts a baseflow response on a much shorter interval than the other methods, making it unsuitable for larger catchments which constitute most of the available data; an increase of storage in baseflow sources should be attenuated, especially in a larger catchment such that a baseflow response occurs more than 1 day after the beginning of a storm event. This method is also more computationally intensive than separation methods 2-4 and requires the calculation of the highly uncertain recession constant. Therefore, I chose not to calculate station BFI values using baseflow separation method 1.

BFI2. The second and third baseflow separation methods were originally developed by Pettyjohn and Henning (1979) and are included in the HYSEP program from Sloto Crouse (1996). Both methods consider a period N, which represents the number of days after which surface runoff ceases. N is calculated using ***Equation 3.1*** where A is the drainage area in square miles.

$$N = A^{0.2} \qquad \textbf{3.1}$$

An interval of $2N^*$ is then calculated as the nearest odd-valued integer between 3 and 11 to two times N. This interval is used to find minimums on the hydrograph. To calculate BFI2, Beck et al. (2015) selected a fixed N of 5 days. This method selects the local minimums within a period of length $2N^*$, 11 days, and connects the minima with straight lines; the baseflow is defined as the area beneath this curve (see the blue curve in ***Figure 3.3***). The code used to calculate BFI2 is presented in *Supplementary S4*.

BFI3. The third baseflow separation method is also calculated using a window of length $2N^*$. Beck et al., (2015) chose an interval length of 7 days, indicating that the chosen N value is between 3 and 4 days. The minimum value on a sliding interval is assigned as the baseflow component for the central value in the interval. The process is repeated across the length of the hydrograph by moving the interval forward in time. This method results in a baseflow curve defined by rectangles of different heights and widths under the hydrograph curve (see the green curve in ***Figure 3.3***, note that they

have linearly connected the rectangles between days, this has no effect on the calculation). The code used to calculate BFI2 is presented in *Supplementary S5*.

The HYSEP program was designed to facilitate automated baseflow separation and improve the consistency of the procedure compared with manual methods (Sloto & Crouse, 1996). Sloto and Crouse (1996) also presented a third baseflow separation method as part of the HYSEP program: the fixed-interval method. This method is calculated by first dividing the streamflow record into intervals of length $2N^*$. The minimum of the interval is assigned as the baseflow value for the interval duration. There is no guidance provided on how and when each of the three methods presented by Sloto and Crouse (1996) should be used. Beck et al. (2015) provide no discussion of their selection of methods 2 and 3 for their global maps, instead of the fixed-interval method of Sloto and Crouse (1996).

BFI4. The fourth baseflow method applied by Beck et al. (2015) was developed by Gustard et al. (1992) to index the effect of geology on low flows in the United Kingdom. BFI4 is calculated by first determining the minimum Q for each 5-day, non-overlapping period. Then, each minimum is compared to its neighbouring minima. If the central minimum is less than 0.9 times the adjacent minima, it is considered an ordinate for the baseflow separation. The ordinates are connected with straight lines across the entire length of the hydrograph. This method effectively combines the local minimum and sliding-interval methods of BFI2 and BFI3. First, flashy peaks are eliminated by determining the minimum of each short period. Then longer peaks are eliminated by comparing neighbouring minima. The resulting baseflow curve is very smooth but rises according to long-term changes in the streamflow. The length of the baseflow rise is defined by the structure of peaks and valleys during the streamflow recession (***Figure 3.3***).

Baseflow separation method 4 is not suitable for application to streams with low, stable discharge and low-resolution records, for example, a stream whose daily values are recorded using integer values less than 10 during the dry season. In this example, it is unlikely for any local minimum to be less than 0.9 times its neighbouring minima. This results in entire sections of the hydrograph being counted as quickflow even when it is likely that low, stable discharge represents baseflow. Many small catchments would have erroneously low BFI4 due to their poor resolution. Therefore, I excluded this

method. Baseflow separation methods 1 and 3, and methods 2 and 4, respectively, produce similar BFI values. The selection of methods 2 and 3, therefore, covers nearly the same range of BFI values as the full set of BFI methods for each station.

3.5 –Flow Routing

I then downscaled the local BFI maps from Beck et al. (2015) to create high-resolution maps of BFI using ArcGIS Pro. I first calculated the total discharge volume (in units of 1000 m^3/year) originating in each cell by multiplying the gridded runoff values (mm/year) by the cell area (km^2) using the raster calculator function. Then, I multiplied the discharge volume by the local BFI values from Beck et al. (2015). I repeated this step for maps of BFI2 and BFI3. During this step, I ensured that the larger cells of the local BFI maps aligned with the smaller cell values of the high-resolution discharge volume layer by setting the spatial extent of the calculated raster to exactly match the extent of the discharge volume layer and adjusting the parameter in ArcGIS Pro to snap the

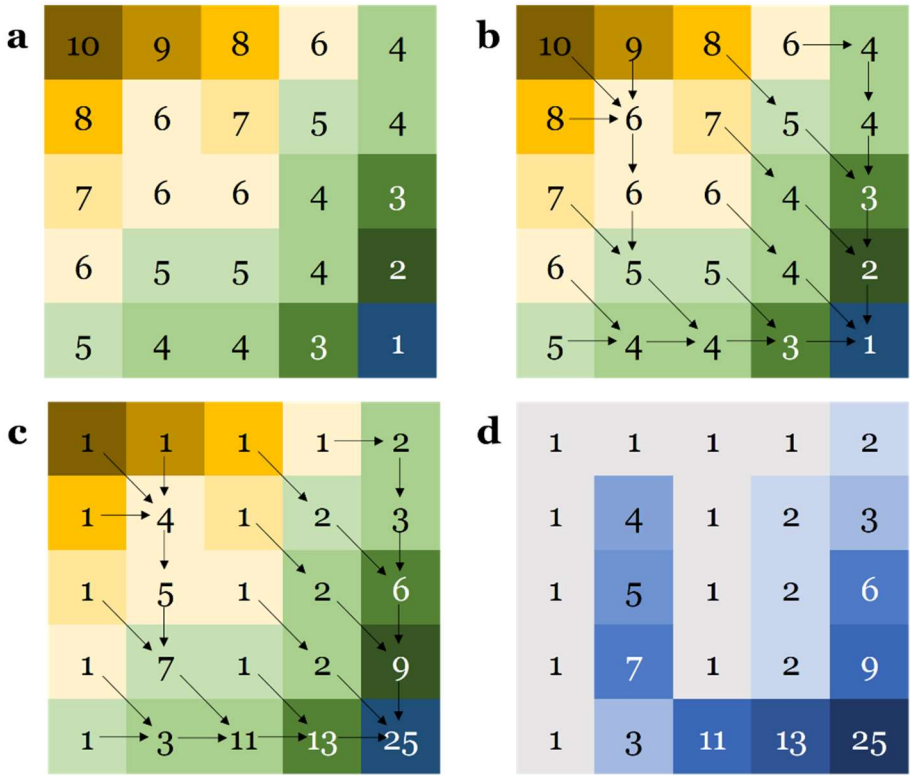

Figure 3.5 *Diagram of flow accumulation in GIS. (**a**) is a digital elevation model (DEM) where each cell value represents the average elevation of the ground surface in the cell. Yellow-brown cells have a higher elevation than green-blue cells. (**b**) the arrows represent the direction of water flow. Water is modelled as flowing downhill into its lowest-valued neighbouring cell. (**c**) the value of the cell represents the cumulative number of cells that are upstream along the flow path of water, including itself. (**d**) The colour of the cell represents the amount of accumulated water in the cell, darker blue cells have a greater volume of accumulated water. In this example, two tributaries are formed and meet in the bottom right corner.*

output raster to the high-resolution input layer. This ensures that the created baseflow volume layer has the same high resolution as the total discharge volume layer. This step accomplishes the direct downscaling of the local BFI maps.

Then, I used the flow accumulation function in ArcGIS Pro to calculate the streamflow and baseflow downstream. The flow accumulation function uses the flow direction map to count the upstream cells whose discharge passes through the cell along the flow path (***Figure 3.5***). Flow accumulation optionally takes a weight layer as input. To calculate streamflow, I used the discharge volume layer as the weight, such that the output layer cell values represent a sum of the discharge volume of the upstream cells. To accumulate baseflow, I used the baseflow volume layer as the weight, creating an accumulated baseflow output for both baseflow methods, 2 and 3. After flow accumulation, I added the weight layer to the accumulated layer for streamflow and baseflow 2 and 3, as flow accumulation does not include a cell's value in the summation of upstream cells. Therefore, a given cell's contribution to streamflow must be added separately using the raster calculator function. Without this step, cells with no upstream contribution will have erroneous zero values.

Then, I replaced all cells with true zero values (zero discharge) in the streamflow layer with an arbitrarily small value, here 1×10^{8}, such that the downscaled BFI – which is calculated by dividing baseflow by streamflow – would not result in null values where the denominator in the calculation is zero. This alteration has no effect on the resulting BFI, as the accumulated baseflow will have zero values in the same pixels, as the baseflow layer is produced through multiplication with the same discharge volume layer that contains zero flow values. I performed the BFI calculation using the raster calculator function to divide the accumulated baseflow in each cell by the corresponding accumulated streamflow value. I repeated this step to produce the routed, downscaled BFI layers for baseflow separation methods 2 and 3 (cartographic model presented in *Supplementary S6*).

3.6 –Validation

The computed BFI2-3 values, here called station BFI2-3, were compared to the BFI2-3 values extracted from the gridded, flow downscaled BFI map, here called downscaled BFI2-3, and the local BFI2-3 extracted from the Beck et al. (2015) maps. After the

downscaled and local BFI2-3 values were extracted from the gridded datasets, I performed a linear regression analysis between station BFI2-3 and downscaled BFI2-3, and between the station BFI2-3 and local BFI2-3. The code used to complete the regressions is presented in *Supplementary S7*.

Chapter 4 – Results

BFI was calculated for all global river reaches in a high-resolution gridded format from a local BFI gridded dataset using flow routing. The resulting map and validation data are presented below.

4.1 –High-Resolution Global BFI Map

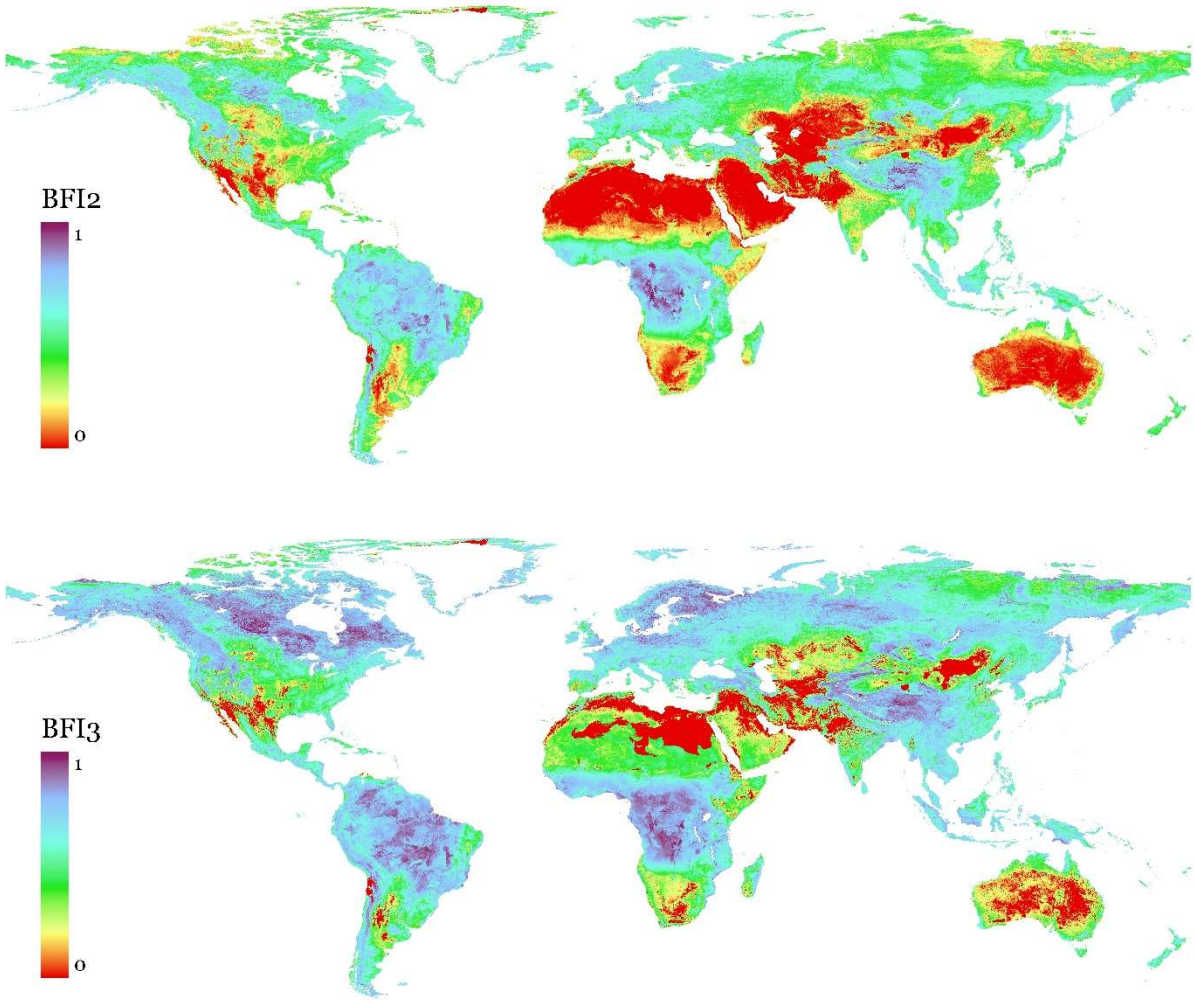

Figure 4.1 *Global Maps of Downscaled, Flow Routed BFI2 and BFI3 on the unglaciated land surface.*

The pattern of river reach BFI very closely resembles the local BFI maps from Beck et al. (2015) at a broad scale (***Figure 4.1***). BFI values are generally spread relatively evenly across latitudes. High BFI values are generally found in the equatorial region (~15°S-10°N) and the high mid-latitudes (~45°N-65°N). High BFI values are also found in

mountain ranges, in the tropics, and the northern tundra zones. Within each river channel, the BFI is most similar to the upstream region and slowly changes with the addition of tributaries in a region with a different average BFI. Headwaters generally have more extreme BFI values which converge toward intermediate values progressing along the river channel. ***Figures 4.2*** and ***4.3a-h*** show the increased resolution achieved using flow routing. The river channel BFI is an average of the local BFI values of each cell in its catchment area, weighted by their contribution to river discharge. Therefore, stream channels are visible on the high-resolution map, as their BFI does not exactly match the local contribution of its floodplains. ***Figure 4.3a-h*** shows sections of the high-resolution, global river reach BFI map. The river reaches are visible when the river reach BFI is much higher or lower than the surrounding local BFIs of the catchment and floodplains. The course resolution local BFI values are reproduced in the high-resolution map in cells with little or no upstream contribution to streamflow.

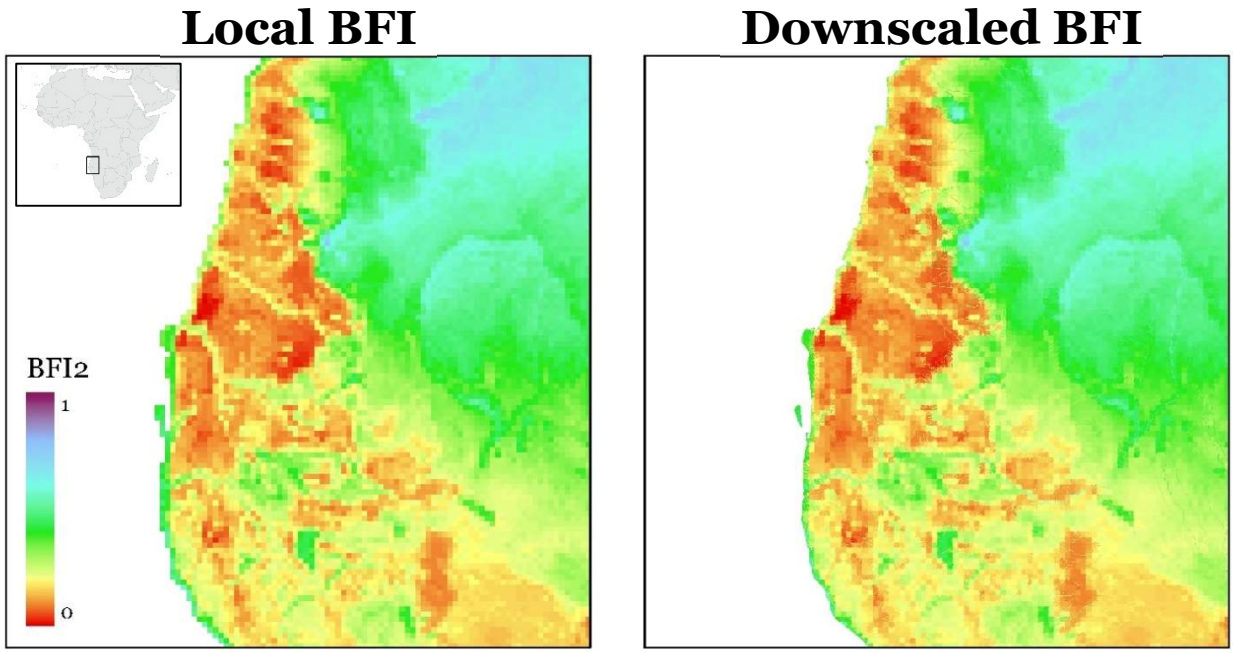

Figure 4.2 *Selected region of southwestern Africa (Namibia and Angola) of the local BFI2 map (Beck et al., 2015) and the downscaled, flow routed BFI2 maps showing the similar pattern of BFI2. In the downscaled BFI map, streams are visible at high-resolution where the stream BFI is not equal to the surrounding local BFI.*

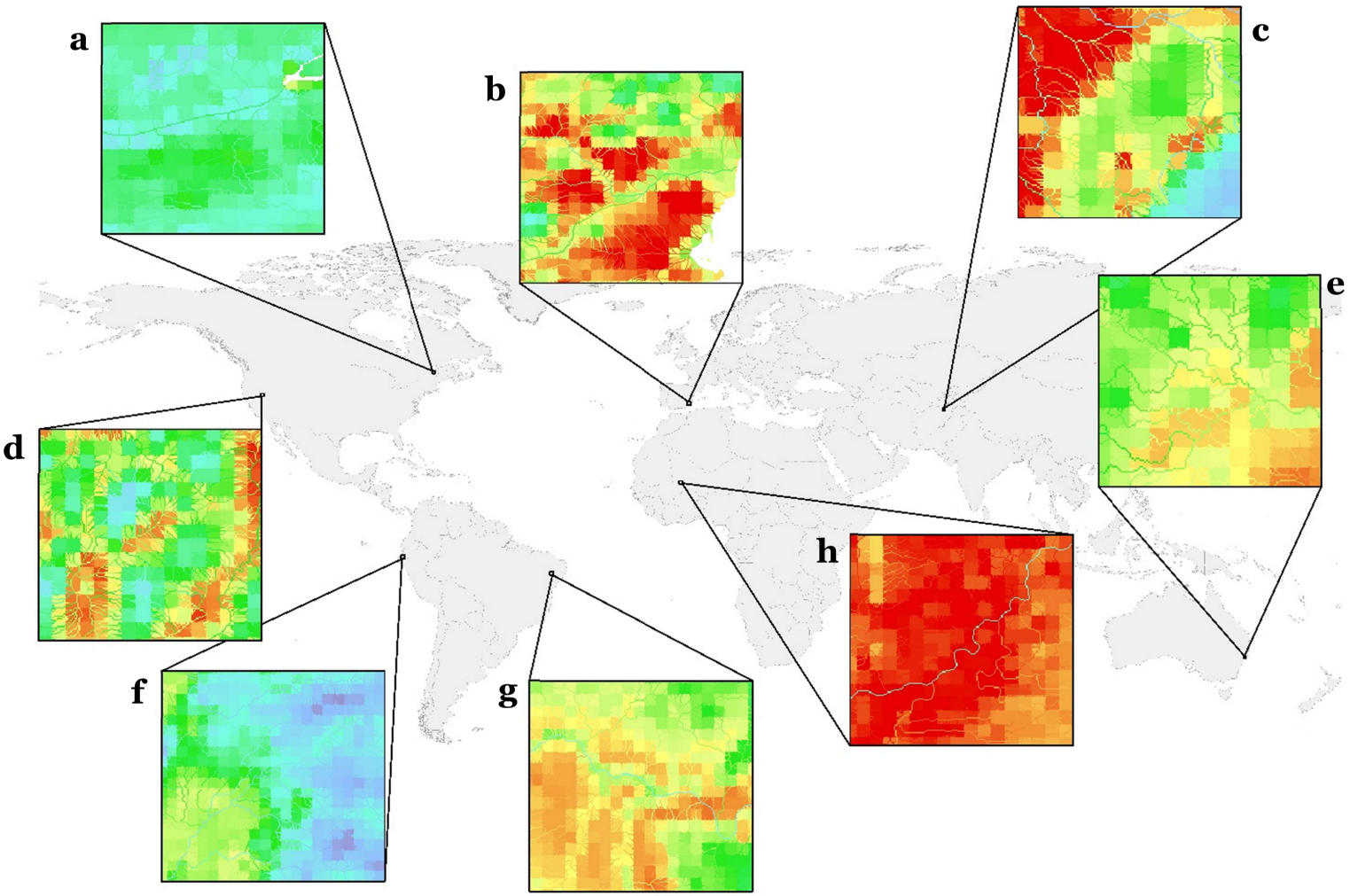

Figure 4.3a-h *Map of selected insets of downscaled, flow routed BFI2 showing high-resolution and river reach BFI patterns. The local BFI, coarse resolution cell values are reproduced in the high-resolution map in cells with few upstream contributing cells. River reaches are highly contrasting where the surrounding local BFI is different from the upstream average BFI, especially in insets* ***b****,* ***c****,* ***e****, and* ***h****. In insets* ***a****,* ***f****, and* ***g****, the surrounding local BFI is similar to the BFI values along the river reaches, causing the streams to be less visible in the inset. Insets* ***b*** *and* ***d*** *depict regions with heterogenous local BFI values. The streams have intermediate BFIs of the surrounding regions.*

4.2 –Validation of Results

Scatterplots of station BFI2-3 and downscaled BFI 2-3 vs. the $\log_{10}$ of the catchment area are shown in ***Figure 4.4a-d***. Greater upstream catchment area is more related to large station BFI2-3 than downscaled BFI2-3. There is no trend in downscaled BFI2-3 vs. catchment area, while there is an increasing trend in station BFI2-3 vs. catchment area. The 95th percentile of downscaled BFI2 is 0.74, and 0.82 for BFI3. The 95th percentile for station BFI2 is 0.87, and 0.94 for BFI3. Station BFI3 has a concentration of points with values between 0.75 and 0.95, especially for upstream catchment areas greater than 10,000 km^2. Station and downscaled BFI2-3 are exclusively greater than 0.5 for catchments larger than 100,000 km^2. Station BFI3 is greater on average than station BFI2, with more points concentration above 0.7 and fewer points below 0.4. In contrast, the difference between downscaled BFI2-3 is less pronounced, although BFI3 is generally slightly greater.

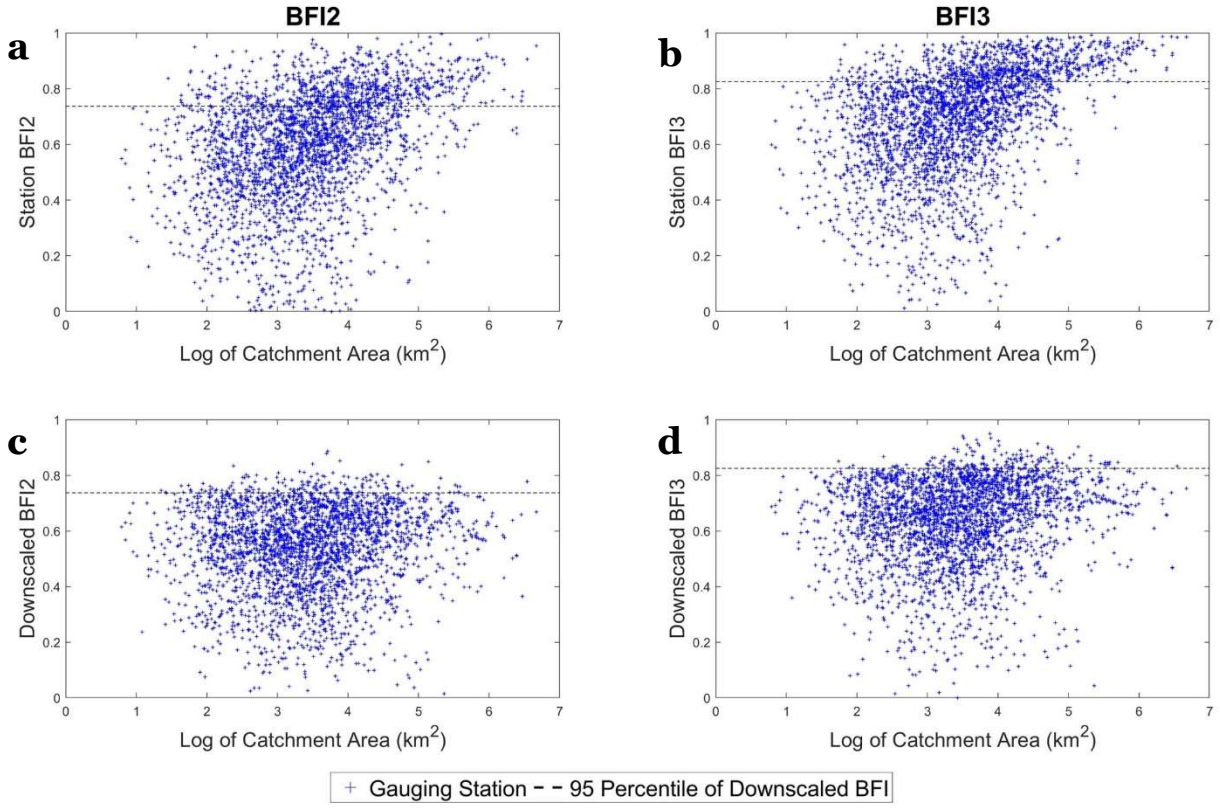

Figure 4.4a-d *Scatterplots of station BFI2-3 and downscaled BFI2-3 vs. Log of catchment area. The dashed black line in* ***a****,* ***b****,* ***c****, and* ***d*** *indicates the 95th percentile of downscaled BFI2-3 for comparison of the range of station and downscaled BFI2-3.*

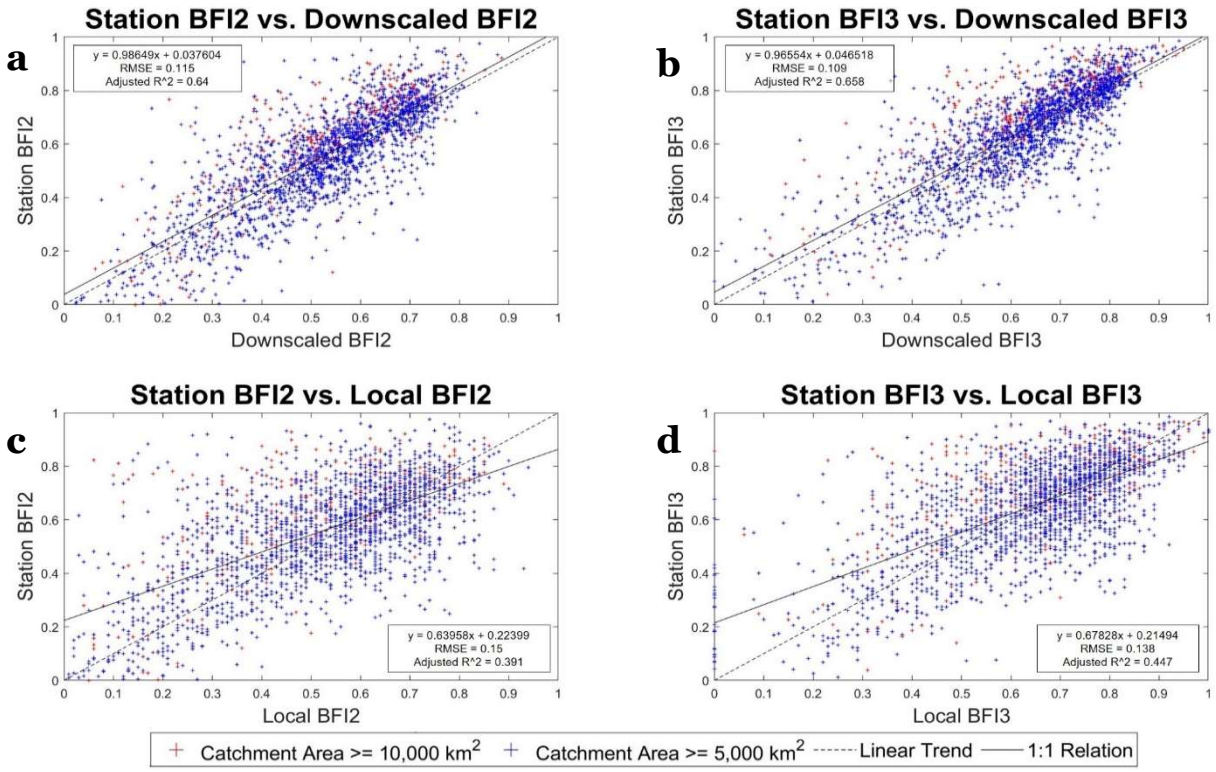

Figure 4.5a-d *Comparison of regression of downscaled BFI2-3 on station BFI2-3 and regression of local BFI2-3 on station BFI2-3. The red points represent gauging stations in catchments with an upstream area greater than or equal to 10,000 km². The blue points represent gauging stations in catchments greater than or equal to 5,000 km². The linear trend is shown as a black line. The 1:1 relation is shown as a dashed line. The equations, root mean square error (RMSE) and adjusted R² are given for each regression in the upper or lower corner.*

Scatterplots of station BFI2-3 vs. downscaled BFI2-3 and station BFI2-3 vs. local BFI2-3 are presented in ***Figure 4.5***. The linear regression is indicated by a solid line and the 1:1 relation by a dashed line. Each data point represents a catchment (n=2,941). The scatterplots show the transformed BFI2-3 to ensure robust regressions for non-normally distributed data. The slope of the regression of the station BFI2-3 on downscaled BFI2-3 are both near unity (BFI2 slope is slightly greater, BFI3 slope is slightly lower). The y-intercepts for all regressions are greater than zero, but the downscaled vs. station intercepts are closer to zero. The linear regression for downscaled vs. station is nearly parallel to the 1:1 relation but is shifted up slightly. The regression using downscaled values has more predictive power for station values than the local BFI from Beck et al. (2015).

The residuals are heteroscedastic for the linear regression of downscaled BFI2-3 on station BFI2-3 (***Figure 4.6***). The residuals are large and positive for downscaled BFI between 0.4 and 0.7 and are large and negative for downscaled BFI between 0 and 0.4 for BFI2 and 0 and 0.55 for BFI3. Small positive and negative residuals are present for BFI2-3 less than 0.4 and BFI2-3 greater than 0.55, respectively. There are very few data points with BFI2-3 Estimated greater than 0.7.

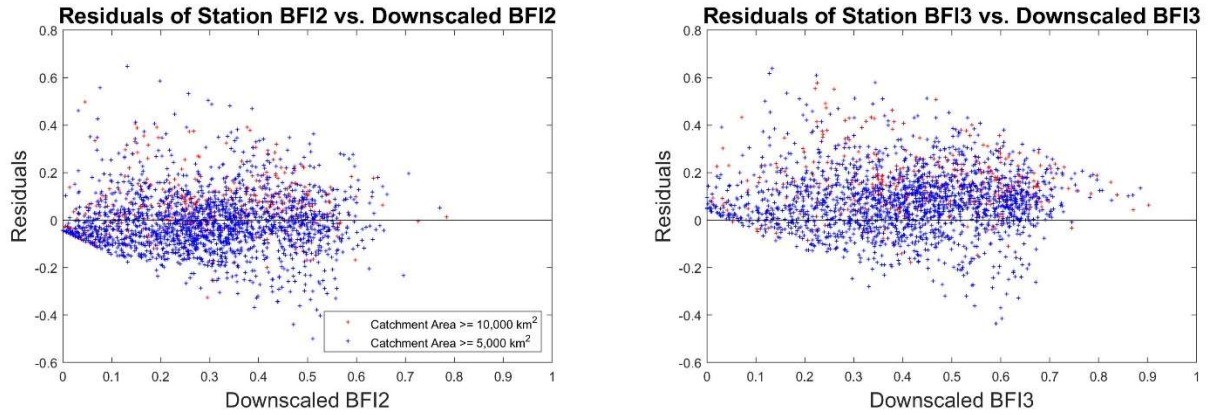

Figure 4.6 *Scatterplot of Residuals of Regression of Downscaled BFI2-3 on Station BFI2-3 . Positive residuals indicate that a gauging station has a greater station BFI2-3 than predicted from its downscaled BFI2-3.*

Chapter 5 –Discussion

5.1 – Evaluation of Selected Baseflow Separation Methods

Every baseflow separation method relies on a set of assumptions about the catchment and/or hydrograph characteristics. The most significant of these assumptions is the definition of baseflow. As discussed in the introduction, a variety of definitions of baseflow are found in the literature. Many studies assume that baseflow is equivalent to groundwater discharge which can be determined from baseflow separation, including Van Dijk (2010), whose method is used to calculate BFI1. Groundwater discharge can be calculated using ***Equations 2.1*** and ***2.2*** for an aquifer given the following assumptions: large, homogenous, uniform, isotropic and specifically bounded unconfined aquifer in a humid environment (Tallaksen, 1995). Halford and Mayer (2000) tested the fundamental assumptions of baseflow separation (see *section 2.1* for the assumptions). They suggest that due to the violation of these assumptions, the prevalence of groundwater discharge outside of rivers, such as evapotranspiration and leakage to deep aquifers, and the contribution of other delayed sources to streamflow, it is not possible to equate groundwater with baseflow calculated using graphical or analytical baseflow separation methods. Halford and Mayer (2000) specifically caution against using baseflow to understand catchment hydrogeologic properties. On a global scale, it is impractical to assess the concordance with the assumptions. Beck et al. (2013) define baseflow in the first line as "the slowly varying portion of streamflow, originating from groundwater storage and/or other delayed sources such as channel banks storage, lakes, wetlands, and melting snow and ice" (p. 7843). This definition excludes applications specific to hydrogeology but still allows the stable portion of streamflow to be characterized and quantified on a global scale without violating the fundamental assumptions of analytical baseflow separation. It is theoretically possible to identify the contributions from multiple sources of baseflow, such as wetlands, lakes, groundwater, and snow- and ice-melt, using additional catchment characteristics, such as the area of wetlands within the catchment, but this is outside the scope of this study.

Another major assumption of graphical or analytical baseflow separation is that the streams analyzed are gaining streams along their entire length and throughout the

year, as BFI is always positive. Gaining streams strictly receive groundwater discharge, compared with losing streams which recharge groundwater. In general, perennial streams are thought to be gaining, while ephemeral streams may be losing (McMahon & Nathan, 2021). Losing streams are also found in arid regions and areas with highly permeable stream beds. Gaining streams may become losing in the dry season if the water table falls sufficiently, or during the flood stage (Fetter, 1988). Groundwater pumping near streams can also increase surface water infiltration by lowering the groundwater head. Globally, it is erroneous to assume that all streams are gaining. Although none of the selected separation methods can return a negative value, losing streams should have very low BFI estimates using all four methods. During flow routing, entering a river reach that is losing should reduce baseflow. However, the false positive BFI for these streams will result in additions to baseflow that increase throughout the losing sections rather than decreasing further. Along the length of the stream, the baseflow estimate will deviate further from the "true" value.

Beck et al. (2015) performed baseflow separation on daily gauge station data. Although daily timescales are thought to be appropriate for baseflow studies (McMahon & Nathan, 2021), there are other complications arising from the hydrograph data. Gauge stations may not be equipped to measure bed flow in streams causing systematic underestimation of streamflow, especially in streams with permeable channel beds. Low flow data quality is often limiting for hydrograph-based analyses (Tallaksen, 1995). The instrumentation used at the gauge stations may have a resolution that is not fine enough to record small streamflow values. On a global scale, the lower limit may not be consistent across the globe, leading to more anomalous zero flow days in some catchments than others. Many of the gauge stations have missing data on days, months, or years during the record. Baseflow methods 2, 3 and 4 can ignore short gaps of fewer than five days, while method 1 is impeded by one day of missing data. Method 1 is also the only method whose application is impacted by zero flow days which are not considered in the recession constant calculation.

5.2 –Evaluation of Source Data

The source data used for flow accumulation each contain their own set of assumptions and limitations. The flow directions map is derived from SRTM elevation data that was upscaled from 3 arc-seconds. Imperfections in the underlying DEM will be transferred to the flow direction map and the downscaled BFI maps.

Runoff data used to produce discharge estimates were tested against approximately 3,000 global gauging stations with good results for long-term averages. However, the authors note large uncertainties for snow, glacier, and wetland-dominated regions and (semi-)arid conditions (Lehner & Grill, 2013). In (semi-)arid regions, depicted streams may represent dry valleys for much of the year. Further, the runoff values are meant to represent natural conditions. The high-resolution BFI maps can be used to investigate sources of anthropogenic manipulation of streamflow that affect baseflow by comparing current conditions with the maps. For instance, groundwater extractions near the river channel can decrease groundwater discharge to streams, leading to a reduced BFI from natural conditions (Theis, 1940), which may be identifiable by comparing BFI in a stream near extensive groundwater pumping to the downscaled BFI maps. The mismatch between natural and anthropogenically altered streamflow may account for some differences between the station BFI and local and downscaled BFI values.

The zero-values in the discharge data result in downscaled BFI representing this zero-value due to the multiplication with the discharge volume layer. In the map of BFI3, the sharp line between zero BFI and intermediate BFI values, especially visible as a red vs. green divide in the northern Sahara is caused by the zero values. Although this region also has zero values in the BFI2 map, the surrounding BFI values are closer to zero, making the transition more gradual. Baseflow method 3 generally has higher values across the globe, therefore, the zero values are more obvious.

5.3 – Evaluation of Local BFI Maps

The global BFI maps from Beck et al. (2015) were used to represent the local BFI index for water derived from each cell. The maps were created by regionalizing catchment climatic and physiographic characteristics from over 3,000 gauging. However, catchments near the maximum area may still contain diverse sub-catchments with

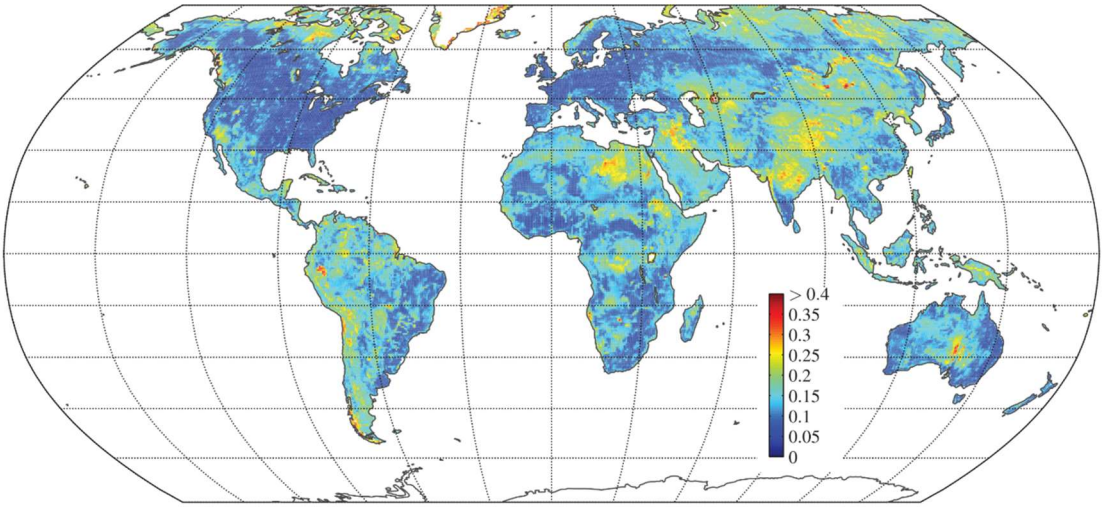

Map 5.1 *Uncertainty in local BFI mapsl (from Beck et al., 2013). The data represent the per-pixel standard deviation of the 10 transformed estimates (one for each cross-validation iteration).*

varied baseflow ratios. Their selected catchments were also concentrated in the global north but excluded arctic regions. Therefore, uncertainties in the underlying local BFI layer are higher in South America, North Africa and South and Central Asia (***Figure 5.1***).

The four baseflow separation methods were developed for and/or tested in a set of catchments in a given region. The characteristics of the testing catchments cannot represent the diversity of global climates. Once applied to Beck et al.'s (2013, 2015) set of over 3,000 gauging stations, the methods are applied to catchment characteristics much different than the set of catchments that the methods were developed for, which may compromise the applicability in some regions. The most significant catchment characteristic is the upland area. Methods 2, 3, and 4 use local-minimum streamflow to separate flashy peaks from the stable portion of streamflow. Method 1 also calculates baseflow as the lower variability portion of streamflow by identifying the hydrograph recession period. Intuitively, these methods should be limited to small catchments; in a large catchment, storm runoff will take longer to reach the gauging station and will experience delays and transmission losses reducing the intensity of the quickflow peak. BFI1 was developed and tested on catchments between 51 and 1780 km^2, much smaller than the 10,000 km^2 maximum imposed by Beck et al. (2013, 2015). The limit of 11 for $2N^*$ suggests that method 2 is designed for catchments less than approximately 13,000 km^2. However, BFI3 is calculated with N between 3 and 4, suggesting a maximum

catchment area of 2,600 km². I calculated these maximum areas using ***Equation 3.1*** and converted the areas into km² from square miles. BFI4 was tested on 865 catchments in the United Kingdom with a maximum area of 8231 km² and a mean area of 284 km² (Gustard et al., 1992). Therefore, the estimated BFI1-4 for a larger catchment may be inflated. Beck et al. (2013) also note this effect and the associated uncertainty in BFI estimates. The upper limit on catchment area in baseflow separation supports the importance of flow routing in this study.

5.4 – Evaluation of High-Resolution BFI Maps

Global maps of BFI at 15 arc-second resolution showed high BFI in humid regions and regions with poor soil drainage (i.e., tundra-taiga) and high mountain regions. Humid regions often have thick soils and available water to facilitate groundwater recharge that contributes to baseflow. Sub-arctic regions may have high baseflow contributions due to snow and ice melt preventing surface water from contributing to streamflow during the long winter months when deep groundwater feeds baseflow and snow- and ice-melt contribute to baseflow as delayed surface water contributions. Mountain block recharge is known to contribute significantly to downstream streamflow, which may explain high BFIs at high altitudes even in (semi-)arid regions (Markovich et al., 2019). Headwaters tend to have more extreme BFI values than downstream flows due to the averaging effect of multiple tributary catchments with different BFI ranges entering the stream. Intermediate BFI values in large rivers occur as their river basins span hundreds to thousands of square kilometres with diverse climatic and physiographic features leading to the averaging of extreme headwater BFIs. Streams derived from regions with very homogenous local baseflow contributions do not show this convergence to intermediate BFI values downstream (see ***Figure 4.3a***).

Further downstream along a river, areas directly adjacent to the main stem of the river may have a significantly different BFI than the main stem itself. The BFI of the main stem reflects the overall contribution area, whereas the surrounding floodplain reflects only the floodplain contribution to baseflow. The global map of BFI3 shows intermediate values in very arid regions, such as the Sahara desert surrounding the zero flow region with 0.0 BFI. Although it is possible for baseflow to contribute to streams in very arid regions, the contribution should be much lower, as there is no excess water

that is stored between rainfall events. Therefore, an intermediate BFI surrounding a region with zero discharge is unlikely and may be erroneous.

Accounting for the many uncertainties in the source data, the local BFI maps, and the assumptions of graphical and analytical baseflow separation methods, the correlation between station BFI2-3 and downscaled BFI2-3 are good, with adjusted R^2 values of 0.64 and 0.658, respectively. Station BFI2-3 for large catchments were concentrated in the upper quartile of BFI values regardless of the catchment size or the corresponding downscaled BFI2-3 (***Figure 4.4***). The high BFI values calculated for large catchments are probably due to the attenuation of streamflow peaks during flow concentration toward the gauging station where discharge was recorded, resulting in a smoother hydrograph and higher calculated BFI values. The "true" baseflow ratio is therefore obstructed by streamflow stability from catchment size. Wetlands or surface water bodies present within the catchment may also increase the observed baseflow values using BFI separation methods 2 and 3. The mismatch between local BFI values from Beck et al. (2015) and station BFI can be attributed to the difference between average upstream BFI and predicted baseflow contributions from within the floodplains or an erroneous baseflow calculation from the daily discharge time series.

For selected baseflow separation methods 2 and 3, the length of the period from which a local minimum is selected controls the predicted response time of the aquifer to changes in water availability. BFI3 is expected to be greater than BFI2 because of the shorter interval, i.e., a minimum value applies for a shorter section of the hydrograph. For peaks lasting more than 11 days (six days), the baseflow component will rise using method 2 (method 3). A faster aquifer response time may be related to the size of the catchment and the aquifer properties. Further research could investigate the appropriateness of different baseflow separation methods based on aquifer and catchment characteristics.

The flow routing method used in this study does not consider transmission losses along the river network; all water that enters a stream is assumed to continue through the length of the river until its outlet. This may lead to overestimations of total streamflow, especially in (semi-)arid regions.

The presented global BFI maps represent a single value averaged across all seasons. Baseflow may vary seasonally, especially in catchments dominated by

snowmelt. Although groundwater stores and other baseflow sources have longer residence times and are thought to have longer response times to surface hydrologic changes, seasonal or yearly recessions generally occur in climates where baseflow stores are replenished seasonally. Beck et al. (2013, 2015) make no mention of baseflow seasonality in the determination of their global BFI maps. The correlation between BFI and catchment climatic and physiographic features may be stronger considering monthly or seasonal BFI. Assessing BFI on shorter time intervals is possible using separation methods 2, 3, and 4 by averaging monthly/seasonal BFI values across every year of the streamflow record. Method 1 may require a monthly/seasonal recession constant to be calculated which may pose a challenge for catchments located in climates that experience daily rainfall in certain months. The annual BFI values presented in the global river reach BFI maps still represent a significant step forward toward greater spatial and temporal resolution baseflow determinations. Although the maps do not represent the full range of baseflow throughout the year, the high correlation between station BFI and downscaled BFI suggests that much of the baseflow attributes of the streams are represented and the maps can be used as a first estimate of global river reach BFI.

Chapter 6 – Conclusion

The goal of this study was to determine the baseflow contribution to every river reach, globally and review baseflow methods. The primary outcomes of this study are:

1. Evaluated the assumptions of baseflow separation for application on a global scale. BFI can be used to assess the stability of low flows in river reaches and the contribution of storm runoff to river reaches, but caution is needed in equating baseflow and groundwater discharge.
2. Determined the baseflow ratio of river reaches in a gridded dataset with 15 arc-second resolution using flow routing. BFI values for large rivers generally have intermediate values averaging out extreme headwater BFI values.
3. Validated the river reach BFI maps against BFI calculated from almost 3,000 gauging stations using graphical baseflow separation methods from Sloto and Crouse (1996). Relationship near unity with adjusted R^2 values of 0.64 and 0.658 for BFI2 and BFI3, respectively for regression of downscaled BFI2-3 on station BFI2-3. This is a good result given the many uncertainties, especially from the local BFI maps and other source data.

Global river reach BFI maps can be used as input data for global climate and hydrological models, especially stream temperature and/or chemistry. To increase the efficacy of baseflow maps especially for temperature models, monthly or seasonal BFI indices could be calculated from long-term streamflow records. The created BFI maps can also be used to assess climate change and the sustainability of anthropogenic withdrawals from baseflow sources as the map models the pre-industrial, natural condition. This study could also be expanded by downscaling BFI methods 1 and 4 from Beck et al. (2015), despite the uncertainties of these method, the inclusion of more estimates of BFI in the river reaches would create a range of BFI values for each cell. The created maps of downscaled and flow downscaled BFI represent the first estimate of river reach BFI and especially of baseflow in medium to large rivers, where graphical and analytical baseflow separation methods are not applicable.

References

Aboelnour, M. A., Engel, B. A., Frisbee, M. D., Gitau, M. W., & Flanagan, D. C. (2021). Impacts of Watershed Physical Properties and Land Use on Baseflow at Regional Scales. *Journal of Hydrology: Regional Studies*, *35*, 100810. https://doi.org/10.1016/j.ejrh.2021.100810

Allen, A., & Chapman, D. (2001). Impacts of afforestation on groundwater resources and quality. *Hydrogeology Journal*, *9*(4), 390–400. https://doi.org/10.1007/s100400100148

Alley, W. M. (2007). Another Water Budget Myth: The Significance of Recoverable Ground Water in Storage. *Groundwater*, *45*(3), 251–251. https://doi.org/10.1111/j.1745-6584.2006.00274.x

Arora, V., Seglenieks, F., Kouwen, N., & Soulis, E. (2001). Scaling aspects of river flow routing. *Hydrological Processes*, *15*(3), 461–477. https://doi.org/10.1002/hyp.161

Barnes, B. S. (1939). The structure of discharge-recession curves. *Eos, Transactions American Geophysical Union*, *20*(4), 721–725. https://doi.org/10.1029/TR020i004p00721

Beck, H. E., Roo, A. de, & Dijk, A. I. J. M. van. (2015). Global Maps of Streamflow Characteristics Based on Observations from Several Thousand Catchments. *Journal of Hydrometeorology*, *16*(4), 1478–1501. https://doi.org/10.1175/JHM-D-14-0155.1

Beck, H. E., van Dijk, A. I. J. M., Miralles, D. G., de Jeu, R. A. M., Sampurno Bruijnzeel, L. A., McVicar, T. R., & Schellekens, J. (2013). Global patterns in base flow index and recession based on streamflow observations from 3394 catchments: Global Patterns in Base Flow Characteristics. *Water Resources Research*, *49*(12), 7843–7863. https://doi.org/10.1002/2013WR013918

Bedient, P. B., Huber, W. C., Vieux, B. E., Mallidu, M., & Huber, W. C. (2013). *Hydrology and floodplain analysis* (5. ed., international ed). Pearson.

Bierkens, M. F. P. (2015). Global hydrology 2015: State, trends, and directions. *Water Resources Research*, *51*(7), 4923–4947. https://doi.org/10.1002/2015WR017173

Briggs, M. A., Johnson, Z. C., Snyder, C. D., Hitt, N. P., Kurylyk, B. L., Lautz, L., Irvine, D. J., Hurley, S. T., & Lane, J. W. (2018). Inferring watershed hydraulics and cold-water habitat persistence using multi-year air and stream temperature signals. *Science of The Total Environment*, *636*, 1117–1127. https://doi.org/10.1016/j.scitotenv.2018.04.344

Döll, P., Kaspar, F., & Lehner, B. (2003). A global hydrological model for deriving water availability indicators: Model tuning and validation. *Journal of Hydrology*, *270*(1), 105–134. https://doi.org/10.1016/S0022-1694(02)00283-4

Eagleson, P. S. (1986). The emergence of global-scale hydrology. *Water Resources Research*, *22*(9S), 6S-14S. https://doi.org/10.1029/WR022i09Sp0006S

Eckhardt, K. (2005). How to construct recursive digital filters for baseflow separation. *Hydrological Processes*, *19*(2), 507–515. https://doi.org/10.1002/hyp.5675

Eckhardt, K. (2008). A comparison of baseflow indices, which were calculated with seven different baseflow separation methods. *Journal of Hydrology*, *352*(1–2), 168–173. https://doi.org/10.1016/j.jhydrol.2008.01.005

Ellison, D., Morris, C. E., Locatelli, B., Sheil, D., Cohen, J., Murdiyarso, D., Gutierrez, V., Noordwijk, M. van, Creed, I. F., Pokorny, J., Gaveau, D., Spracklen, D. V., Tobella, A. B., Ilstedt, U., Teuling, A. J., Gebrehiwot, S. G., Sands, D. C., Muys, B., Verbist, B., … Sullivan, C. A. (2017). Trees, forests and water: Cool insights for a hot world. *Global Environmental Change*, 43, 51–61. https://doi.org/10.1016/j.gloenvcha.2017.01.002

Fekete, B., & Vörösmarty, C. (2002). The current status of global river discharge monitoring and potential new technologies complementing traditional discharge measurements. *Proceedings of the PUB Kick-off Meeting*, *309*, 20–22.

Fetter, C. W. (1988). *Applied hydrogeology* (2nd ed). Merrill Pub. Co.

Gustard, A., Bullock, A., & Dixon, J. M. (1992). *Low flow estimation in the United Kingdom*. Institute of Hydrology.

Halford, K., & Mayer, G. (2000). Problems Associated With Estimating Ground Water Discharge and Recharge From Stream-Discharge Records. *Ground Water*, *38*, 331–342. https://doi.org/10.1111/j.1745-6584.2000.tb00218.x

Hall, F. R. (1968). Base-Flow Recessions—A Review. *Water Resources Research*, *4*(5), 973–983. https://doi.org/10.1029/WR004i005p00973

Khan, M. R., Michael, H. A., Bresnyan, E. W., & Yu, W. (2022). Impacts of basin-wide irrigation pumping on dry-period stream baseflow in an alluvial aquifer in the Kosi Fan region of India and Nepal. *Hydrogeology Journal*, *30*(6), 1899–1910. https://doi.org/10.1007/s10040-022-02527-z

Kissel, M., & Schmalz, B. (2020). Comparison of Baseflow separation Methods in the German Low Mountain Range. *Water*, *12*, 1740. https://doi.org/10.3390/w12061740

Koskelo, A. I., Fisher, T. R., Utz, R. M., & Jordan, T. E. (2012). A new precipitation-based method of baseflow separation and event identification for small watersheds (<50km2). *Journal of Hydrology*, *450–451*, 267–278. https://doi.org/10.1016/j.jhydrol.2012.04.055

Lehner, B., & Grill, G. (2013). Global river hydrography and network routing: Baseline data and new approaches to study the world's large river systems. *Hydrological Processes*, *27*(15), 2171–2186. https://doi.org/10.1002/hyp.9740

Lehner, B. (2012). Derivation of watershed boundaries for GRDC gauging stations based on the HydroSHEDS drainage network. Tech. Rep. 41, Global Runoff Data Centre, Federal Institute of Hydrology, Koblenz, Germany, 12.

Linke, S., Lehner, B., Ouellet Dallaire, C., Ariwi, J., Grill, G., Anand, M., Beames, P., Burchard-Levine, V., Maxwell, S., Moidu, H., Tan, F., & Thieme, M. (2019). Global hydro-environmental sub-basin and river reach characteristics at high spatial resolution. *Scientific Data*, 6(1), 283. https://doi.org/10.1038/s41597-019-0300-6

Longobardi, A., & Villani, P. (2008). Baseflow index regionalization analysis in a mediterranean area and data scarcity context: Role of the catchment permeability index. *Journal of Hydrology*, *355*(1), 63–75. https://doi.org/10.1016/j.jhydrol.2008.03.011

Lott, D. A., & Stewart, M. T. (2016). Base flow separation: A comparison of analytical and mass balance methods. *Journal of Hydrology*, *535*, 525–533. https://doi.org/10.1016/j.jhydrol.2016.01.063

Markovich, K. H., Manning, A. H., Condon, L. E., & McIntosh, J. C. (2019). Mountain-Block Recharge: A Review of Current Understanding. *Water Resources Research*, *55*(11), 8278–8304. https://doi.org/10.1029/2019WR025676

McMahon, T. A., & Nathan, R. J. (2021). Baseflow and transmission loss: A review. *WIREs Water*, *8*(4), e1527. https://doi.org/10.1002/wat2.1527

Miller, M. P., Buto, S. G., Susong, D. D., & Rumsey, C. A. (2016). The importance of base flow in sustaining surface water flow in the Upper Colorado River Basin. *Water Resources Research*, *52*(5), 3547–3562. https://doi.org/10.1002/2015WR017963

Mukherjee, A., Bhanja, S. N., & Wada, Y. (2018). Groundwater depletion causing reduction of baseflow triggering Ganges river summer drying. *Scientific Reports*, *8*(1), 1–9. https://doi.org/10.1038/s41598-018-30246-7

Partington, D., Brunner, P., Simmons, C. T., Werner, A. D., Therrien, R., Maier, H. R., & Dandy, G. C. (2012). Evaluation of outputs from automated baseflow separation methods against simulated baseflow from a physically based, surface water-groundwater flow model. *Journal of Hydrology*, *458–459*, 28–39. https://doi.org/10.1016/j.jhydrol.2012.06.029

Peña-Arancibia, J. L., van Dijk, A. I. J. M., Mulligan, M., & Bruijnzeel, L. A. (2010). The role of climatic and terrain attributes in estimating baseflow recession in tropical catchments. *Hydrology and Earth System Sciences*, *14*(11), 2193–2205. https://doi.org/10.5194/hess-14-2193-2010

Peralta-Tapia, A., Sponseller, R. A., Ågren, A., Tetzlaff, D., Soulsby, C., & Laudon, H. (2015). Scale-dependent groundwater contributions influence patterns of winter baseflow stream chemistry in boreal catchments. *Journal of Geophysical Research: Biogeosciences*, *120*(5), 847–858. https://doi.org/10.1002/2014JG002878

Pettyjohn, W. A., & Henning, R. (1979). Preliminary estimate of ground-water recharge rates, related streamflow and water quality in Ohio. *Ohio State University Water Resources Center Project Completion Report*, *552*.

Reynolds, B., Neal, C., Hornung, M., & Stevens, P. A. (1986). Baseflow buffering of streamwater acidity in five mid-Wales catchments. *Journal of Hydrology*, *87*(1), 167–185. https://doi.org/10.1016/0022-1694(86)90121-6

Richts, A., Struckmeier, W. F., & Zaepke, M. (2011). WHYMAP and the Groundwater Resources Map of the World 1:25,000,000. In J. A. A. Jones (Ed.), *Sustaining Groundwater Resources: A Critical Element in the Global Water Crisis* (pp. 159–173). Springer Netherlands. https://doi.org/10.1007/978-90-481-3426-7_10

Santhi, C., Allen, P. M., Muttiah, R. S., Arnold, J. G., & Tuppad, P. (2008). Regional estimation of base flow for the conterminous United States by hydrologic landscape regions. *Journal of Hydrology*, *351*(1), 139–153. https://doi.org/10.1016/j.jhydrol.2007.12.018

Schilling, K. E., & Libra, R. D. (2003). Increased Baseflow in Iowa Over the Second Half of the 20th Century1. *JAWRA Journal of the American Water Resources Association*, *39*(4), 851–860. https://doi.org/10.1111/j.1752-1688.2003.tb04410.x

Schneider, M. K., Brunner, F., Hollis, J. M., & Stamm, C. (2007). Towards a hydrological classification of European soils: Preliminary test of its predictive power for the base flow index using river discharge data. *Hydrology and Earth System Sciences*, *11*(4), 1501–1513. https://doi.org/10.5194/hess-11-1501-2007

Sloto, R. A., & Crouse, M. Y. (1996). HYSEP: A Computer Program for Streamflow Hydrograph Separation and Analysis. In *Water-Resources Investigations Report* (No. 96–4040). U.S. Geological Survey. https://doi.org/10.3133/wri964040

Stewart, M., Cimino, J., & Ross, M. (2007). Calibration of Base Flow Separation Methods with Streamflow Conductivity. *Groundwater*, *45*(1), 17–27. https://doi.org/10.1111/j.1745-6584.2006.00263.x

Tallaksen, L. M. (1995). A review of baseflow recession analysis. *Journal of Hydrology*, *165*(1–4), 349–370. https://doi.org/10.1016/0022-1694(94)02540-R

Tan, X., Liu, B., & Tan, X. (2020). Global Changes in Baseflow Under the Impacts of Changing Climate and Vegetation. *Water Resources Research*, *56*(9), e2020WR027349. https://doi.org/10.1029/2020WR027349

Theis, C. V. (1940). The source of water derived from wells. *Civil Engineering*, *10*(5), 277–280.

van Dijk, A. I. J. M. (2010). Climate and terrain factors explaining streamflow response and recession in Australian catchments. *Hydrology and Earth System Sciences*, *14*(1), 159–169. https://doi.org/10.5194/hess-14-159-2010

Vogel, R. M., & Kroll, C. N. (1996). Estimation of baseflow recession constants. *Water Resources Management*, *10*(4), 303–320. https://doi.org/10.1007/BF00508898

Wang, Z., Sun, S., Wang, G., & Song, C. (2023). Determination of low-flow components in alpine permafrost rivers. *Journal of Hydrology*, 617, 128886. https://doi.org/10.1016/j.jhydrol.2022.128886

Weinmann, P. E., & Laurenson, E. M. (1979). Approximate Flood Routing Methods: A Review. *Journal of the Hydraulics Division*, 105(12), 1521–1536. https://doi.org/10.1061/JYCEAJ.0005329

Wolock, D. M. (2003). Base-Flow Index Grid for the Conterminous United States. In *Base-Flow Index Grid for the Conterminous United States* (USGS Numbered Series No. 2003–263; Open-File Report, Vols. 2003–263). https://doi.org/10.3133/ofr03263

Zektser, I. S., & Loaiciga, H. A. (1993). Groundwater fluxes in the global hydrologic cycle: Past, present and future. *Journal of Hydrology*, *144*(1–4), 405–427. https://doi.org/10.1016/0022-1694(93)90182-9

Supplementary Materials

S1 – Get Filenames Function

```
# import needed library
import os.path

def get_filenames(min: int, max: int):
    '''
    method takes the minimum and maximum station IDs as input
    returns a list of valid station IDs that serve as gauge station data filenames
    '''
    filenames = range(min,max+1,1) # list of all possible station IDs between min and max
    names = [] # list to store valid station IDs

    # check each possible station ID to find valid station IDs
    for file in filenames:
        if (os.path.isfile(str(file)+'.txt')):
            names.append(file)

    # return the list of valid station IDs
    return names
```

S2 – Load Data Function

```
# import needed
import pandas as pd

def load_data(filenames: list):
    '''
    methods takes a list of station IDs as input
    returns dictionary where each entry maps the
    station number to a dataframe including the data

    note: should be used in conjunction with get_filenames method
    to avoid calling filenames that do not exist
    '''

    data = {} # dictionary to store dataframes

    # iterate over the filenames
    for file in filenames:

        # due to formatting error in station data
        # streamflow data is stored in col 2, except for station IDs
        # beginning with 5
        if file >= 5000000 and file < 6000000:
            col = 3
        else:
            col = 2

        # read the file into the data frame
        df = pd.read_csv(
            filepath_or_buffer= open(str(file)+'.txt','r'),
            delimiter = ';',
            header = 40, # skip 40 lines of header text in input files
            usecols = [0,col],
            parse_dates = [0],
            infer_datetime_format = True,
            )
        df.columns = ['Date','Original'] # column names
```

```
        # add dataframe to dictionary with station ID as key
        data[file] = df

    return data
```

S3 – Fill Gaps Function

```
def fill_gaps(d):
    '''
    method takes a dataframe of streamflow as input
    returns a list of continuous periods of streamflow as dataframes

    streamflow records must have at least 10 years of consecutive data
    with gaps of five days or shorter, making up less than 10% of the data period
    '''
    data = [] # list of consecutive data periods

    c = 0 # number of consecutive days
    n = 0 # number of NaNs

    beg = [] # index of first day in the consecutive data period
    end = []

    thresh = 10 # years of consecutive data needed

    prev_val = float('nan') # last non-NaN value
    prev_i = -1 # last non-NaN index

    # data gaps are linearly interpolated, the values to update are stored here
    values = [] # values to update
    ind = [] # indices to update

    # iterate over each line in the datafram
    # i is the row index, r is the row values (date,discharge)
    for i,r in d.iterrows():
        # if not the first row in the dataframe
        if r['Original'] >= 0:

            # if no previously stored value
            if prev_i == -1:
                prev_val = r['Original'] # set previously value to current value
                prev_i = i
                c += 1

                beg.append(i) # set current index to the beg of period
                continue # move to next row

            # if there are NaNs between the previous and current values
            if i > prev_i + 1 and prev_i != -1:
                diff_i = i - prev_i # number consecutive NaN values

                # if 5 or fewer NaN values in a row
                if diff_i < 7:
                    # linearly interpolate the missing values
                    slope = (r['Original'] - prev_val)/(diff_i)
                    while diff_i > 1:
                        n += 1
                        c += 1
                        diff_i -= 1

                        # values are stored to be updated in the data frame later
```

```
                    ind.append(prev_i + diff_i)
                    values.append(prev_val + slope*diff_i)

            # if more than 5 NaNs in a row
            else:
                # if there are already 10 years of continuous data
                # with less than 10% NaNs
                if c > 365*thresh and n <= round(c*0.1):
                    end.append(prev_i) # record end of continuous period
                    prev_i = i
                    prev_val = r['Original']
                    c = 1
                    n = 0
                    beg.append(i) # record start of new continuous period
                    continue # move to next row in datafram

                # if there are not yet 10 years of continuous data
                else:
                    beg.pop(len(beg) - 1) # remove recorded beg of continous period
                    prev_i = i
                    prev_val = r['Original']
                    c = 1
                    n = 0
                    beg.append(i) # record start of new continous period
                    continue # move to next row in datafram

        # if there are no NaNs between previous and current row
        prev_val = r['Original']
        prev_i = i
        c += 1

    # skip first row
    else:
        continue

# if final data period meets the criteria
if c > 365*thresh and n <= round(c*0.1):
    end.append(prev_i + 1) # record end of consecutive data period

# if final data period does not meet the criteria
else:
    beg.pop(len(beg) - 1)

# fill data gaps
if len(beg) > 0:
    for x in range(len(ind)):
        d.at[ind[x],'Original'] = values[x]

# if suitable consecutive data periods were found,
# add them to the list of consecutive data periods to be returned
for j in range(len(beg)):
    data.append(d.iloc[beg[j]:end[j]].reset_index(drop=True))
return data # return list of consecutive data periods as dataframe
```

S4 – Baseflow Separation Method 2

```
# load functions from external files
from get_filenames import get_filenames
from load_data import load_data
from fill_gaps import fill_gaps

# load isnan method from math library
from math import isnan

# call function to get list of stations IDs, used as filenames
stations = get_filenames(1104150,6997200)

# call function to load station data to dataframe format
# stations stored in a dictionary with key as station name
ad = load_data(stations)

# BFI2 data for stations is stored to a csv file
outputfile = "bfi2_final_v2.csv"
f = open(outputfile, 'a')

# for each station in the dict, s is the number index of the station ID in station name list
for s in range(len(stations)):
    station = stations[s] # station ID

    # 'data' is station data, stored as list of dataframes for each consecutive period of data
    data = ad.get(station)

    # call function to fill short gaps and break data into continuous periods
    # 'data' is corrected dataframe with station data
    data = fill_gaps(ad.get(station))

    # if there are no periods of data of acceptable length
    if len(data) == 0:
        # f.write(str(station) + ',NaN\n') # optionally write 'NaN' to .csv
        continue # go to the next station

    # baseflow and streamflow totals are calculated continously across all data periods
    bflow = 0
    sflow = 0

    # for consecutive period of data within the streamflow record
    for d in data:

        lm_val = float('nan') # local minimum value, initiated as NaN
        lm_i = 0 # local minumum index, initiated as 0
        window = [] # list of streamflow values to store consideration period to find local min
        period = [] # list of streamflow values to store values btw local mins before processing

        # for day in streamflow record, row of dataframe
        # each row has the date and observed streamflow
        for i,r in d.iterrows(): # i is the index of the row, r is the row values

            # add the first 11 values to the window to find the first local minumum
            if i < 11:
                window.append(r['Original'])
                continue

            # if there is no previous local minimum
            if isnan(lm_val):
                # if the middle day of the 11 day window is the local minumum
                if window[5] == min(window):
```

```
                    lm_val = window[5] # set middle-day value as the local minumum
                    lm_i = i - 6 # set the middle-day index as the local minumum index

                    bflow += window[5] # add the local minumum amount to the baseflow total
                    sflow += window[5] # and the streamflow total

                    # shift the window to the next day
                    window.append(r['Original'])
                    window.pop(0)

                # if the middle-day is not the local minimum
                else:
                    # shift the window to the next day
                    window.append(r['Original'])
                    window.pop(0)

            # if there is a previously stored local minimum
            # add baseflow and streamflow to totals from between past and current local mins
            else:
                # if the middle day of the 11-day window is the local minuum
                if window[5] == min(window):
                    diff_i = i - lm_i - 6 # count the number of days between local mins
                    diff_value = window[5] - lm_val # difference btw past and current local mins
                    slope = diff_value/diff_i # rate of inc/dec of baseflow between local mins

                    # if last local min was not previous day
                    while diff_i > 1:
                        diff_i -= 1 # reduce the counter variable
                        cur_val = period[-1] # consider value at the end of period btw local mins

                        # baseflow is linearly interpolated between local mins
                        # baseflow cannot be greater than streamflow on a given day
                        bflow += min(lm_val + (slope*diff_i), cur_val)
                        sflow += cur_val

                        period.pop(-1) # this data point has been accounted for

                    lm_val = window[5] # set middle day to local min
                    lm_i = lm_i = i - 6 # set middle day index to local min index

                    # add current value to baseflow and streamflow totals
                    bflow += window[5]
                    sflow += window[5]

                    # shift the window
                    window.append(r['Original'])
                    window.pop(0)

                # if the middle day is not a local minimum
                else:
                    period.append(window[5]) # add middle day to list of values btw local mins

                    # shift the window
                    window.append(r['Original'])
                    window.pop(0)

    # if the bfi has been successfully calculated
    if sflow != 0:
        f.write(str(station)+","+ str(bflow/sflow) + '\n')
        print(station) # print to terminal to record processing progress

    # if the bfi has not been successfully calculated
```

```
    else:
        print(station) # print to terminal to record processing progress
        # f.write(str(station) + ',NaN\n') # optionally record failure
        # of station as 'NaN' in .csv output
f.close()
```

S5 – Baseflow Separation Method 3

```
# load functions from external files
from get_filenames import get_filenames
from load_data import load_data
from fill_gaps import fill_gaps

# call function to get list of stations IDs, used as filenames
stations = get_filenames(1104150,6997200)

# call function to load station data to dataframe format
# stations stored in a dictionary with key as station name
ad = load_data(stations)

# BFI3 data for stations is stored to a csv file
outputfile = "bfi3_final.txt"
f = open(outputfile, 'a')

# for each station in the dict, s is the number index of the station ID in station name list
for s in range(len(stations)):
    station = stations[s] # station ID

    # 'data' is station data, stored as list of dataframes for each consecutive period of data
    data = ad.get(station)

    # call function to fill short gaps and break data into continuous periods
    # 'data' is corrected dataframe with station data
    data = fill_gaps(ad.get(station))

    # if there are no periods of data of acceptable length
    if len(data) == 0:
        f.write(str(station) + ',NaN\n') # optionally write 'NaN' to .csv
        continue # go to the next station

    # baseflow and streamflow totals are calculated continously across all data periods
    bflow = 0
    sflow = 0

    # for consecutive period of data within the streamflow record
    for d in data:

        # list of streamflow values to store period of consideration to locate local minimum
        window = []

        for i,r in d.iterrows():
            # i is the index of the row
            # r is the row values
            if i == 0: # first row
                # prev_date = r['Date']
                window.append(r['Original'])
                continue

            # add the first 7 rows to the window
            if len(window) < 7:
                window.append(r['Original'])
```

```
                # once the window is full
                # baseflow is the window minimum for each day
                if len(window) == 7:
                    bflow += min(window)
                    sflow += window[3]
                continue # move to next row

            # shift window
            window.append(r['Original'])
            window.pop(0)

            # baseflow is the window minimum for each day
            bflow += min(window)
            sflow += window[3]

    # if BFI calculation was successful
    # record BFI3 in .csv
    if sflow != 0:
        f.write(str(station)+","+ str(bflow/sflow) + '\n')
        print(station) # print to terminal to report progress

    # if BFI calculation was not successful
    else:
        f.write(str(station) + ',NaN\n') # optionally record NaN value in .csv
        print(station) # print to terminal to report progress

f.close()
```

S6 – Cartographic Model

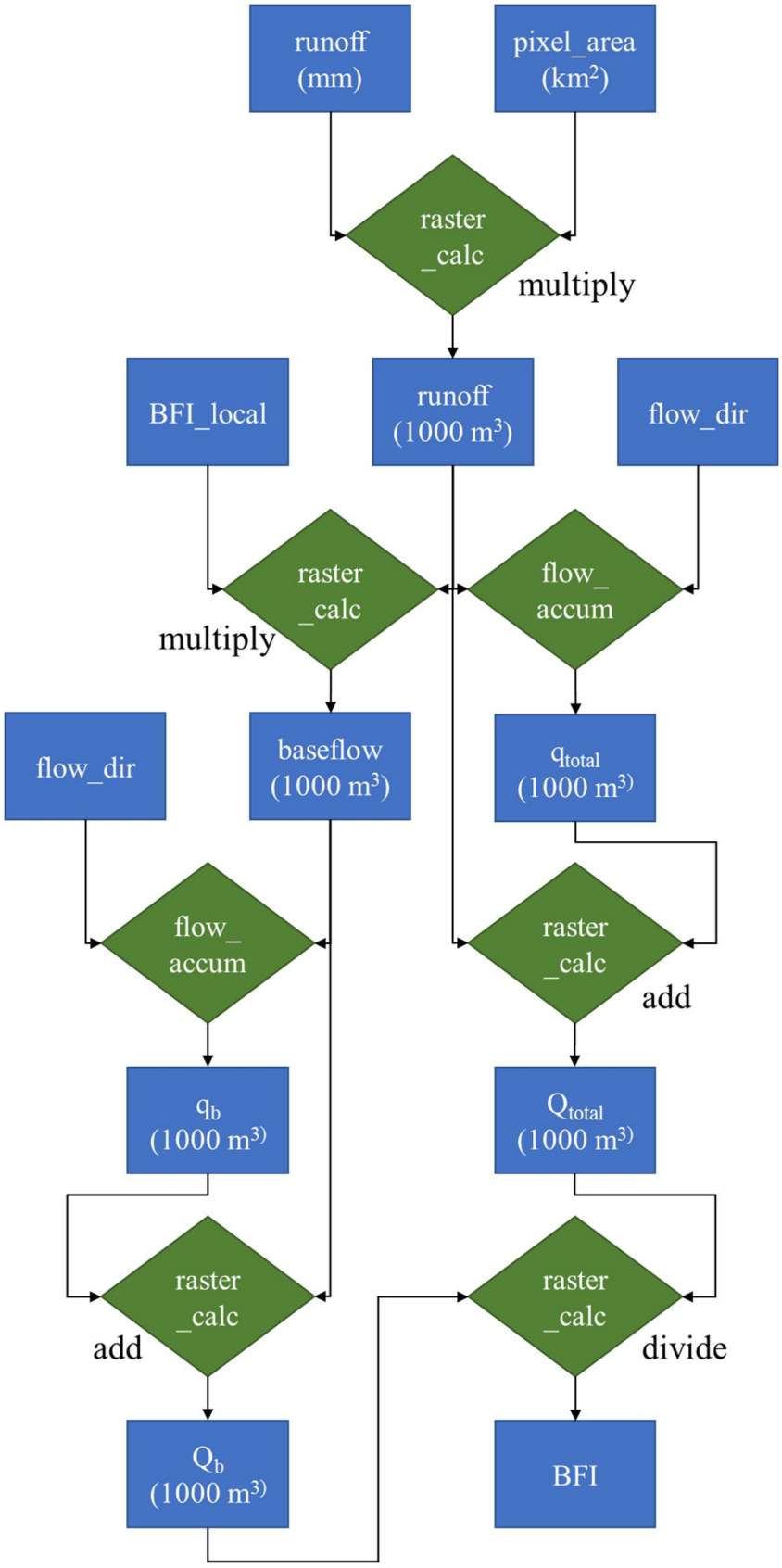

S7 – Regression and Figures

```
%% Load Data

stationsBFI2 = load('BFI2.mat').stationsBFI2;
BFI2_calc = stationsBFI2(:,28);
BFI2_map = stationsBFI2(:,30);
BFI2_area = stationsBFI2(:,7);
BFI2_local = stationsBFI2(:,31);
BFI2_yrs = stationsBFI2(:,6);

stationsBFI3 = load('BFI3.mat').stationsBFI3v2;
BFI3_calc = stationsBFI3(:,28);
BFI3_map = stationsBFI3(:,30);
BFI3_local = stationsBFI3(:,31);
BFI3_area = stationsBFI3(:,7);

x = [0 1];
y = [0 1];

%% Translation

%translate all of the BFI
BFI2t_calc = BFI2_calc.*BFI2_calc;
BFI2t_map = BFI2_map.*BFI2_map;
BFI2t_local = BFI2_local.*BFI2_local;

BFI3t_calc = BFI3_calc.*BFI3_calc;
BFI3t_map = BFI3_map.*BFI3_map;
BFI3t_local = BFI3_local.*BFI3_local;

%% Compare BFI map and BFI calc (catchment <= 10000 km^2)

% BFI2 calc vs. BFI2 map (catchment <= 10000 km^2)
figure(1)

subplot(2,2,1)
BFI2_m2 = fitlm(BFI2t_map(BFI2_area <= 10000), BFI2t_calc(BFI2_area <= 10000))
BFI2_m2_p = polyfit(BFI2t_map(BFI2_area <= 10000),BFI2t_calc(BFI2_area <= 10000),1);
% y = 1.0076x + 0.043284
% RMSE = 0.124
% R^2 = 0.601
plot(BFI2t_map(BFI2_area <= 10000), BFI2t_calc(BFI2_area <= 10000),'r+','MarkerSize',3), hold on
plot(BFI2t_map(BFI2_area <= 5000), BFI2t_calc(BFI2_area <= 5000),'b+','MarkerSize',3)
plot(x, y*BFI2_m2_p(1)+BFI2_m2_p(2),'k')
plot([0 1],[0 1],'--k'), hold off
ylim([0 1]), xlim([0 1])
xlabel('Downscaled BFI2','FontSize',16)
ylabel('Station BFI2','FontSize',16)
title('Station BFI2 vs. Downscaled BFI2','FontSize', 22)
legend('Catchment Area >= 10,000 km^2','Catchment Area >= 5,000 km^2','Linear Trend','1:1
Relation','Location','southeast')

% BFI3 calc vs. BFI3 map (catchment <= 10000 km^2)
subplot(2,2,2)
BFI3_m2 = fitlm(BFI3t_map(BFI3_area <= 10000), BFI3t_calc(BFI3_area <= 10000))
BFI3_m2_p = polyfit(BFI3t_map(BFI3_area <= 10000),BFI3t_calc(BFI3_area <= 10000),1);
% y = 0.99471x + 0.044134
% RMSE = 0.13
% R^2 = 0.64
plot(BFI3t_map(BFI3_area <= 10000), BFI3t_calc(BFI3_area <= 10000),'r+','MarkerSize',3), hold on
plot(BFI3t_map(BFI3_area <= 5000), BFI3t_calc(BFI3_area <= 5000),'b+','MarkerSize',3)
```

```
plot([0 1],[0 1],'--k')
plot(x, y*BFI3_m2_p(1)+BFI3_m2_p(2),'k'), hold off
ylim([0 1]), xlim([0 1])
xlabel('Downscaled BFI3','FontSize',16)
ylabel('Station BFI3','FontSize',16)
title('Station BFI3 vs. Downscaled BFI3','FontSize', 22)

% BFI2 Local vs BFI2 Estimated (catchments <= 10000 km^2)
subplot(2,2,3)
BFI2_m7 = fitlm(BFI2t_local(BFI2_area <= 10000), BFI2t_calc(BFI2_area <= 10000))
BFI2_m7_p = polyfit(BFI2t_local(BFI2_area <= 10000),BFI2t_calc(BFI2_area <= 10000),1);
% y = 0.6122x + 0.15934
% RMSE = 0.163
% R^2 = 0.314
plot(BFI2t_local(BFI2_area <= 10000), BFI2t_calc(BFI2_area <= 10000),'r+','MarkerSize',3), hold
on
plot(BFI2t_local(BFI2_area <= 5000), BFI2t_calc(BFI2_area <= 5000),'b+','MarkerSize',3)
plot([0 1],[0 1],'--k')
plot(x, y*BFI2_m7_p(1)+BFI2_m7_p(2),'k'), hold off
ylim([0 1]), xlim([0 1])
xlabel('Local BFI2','FontSize',16)
ylabel('Station BFI2','FontSize',16)
title('Station BFI2 vs. Local BFI2','FontSize', 22)

% BFI2 Observed vs. BFI2 Local(catchments <= 10000 km^2)
subplot(2,2,4)
BFI3_m7 = fitlm(BFI3t_local(BFI3_area <= 10000), BFI3t_calc(BFI3_area <= 10000))
BFI3_m7_p = polyfit(BFI3t_local(BFI3_area <= 10000),BFI3t_calc(BFI3_area <= 10000),1);
% y = 0.67002x + 0.15872
% RMSE = 0.167
% R^2 = 0.404
plot(BFI3t_local(BFI3_area <= 10000), BFI3t_calc(BFI3_area <= 10000),'r+','MarkerSize',3), hold
on
plot(BFI3t_local(BFI3_area <= 5000), BFI3t_calc(BFI3_area <= 5000),'b+','MarkerSize',3)
plot([0 1],[0 1],'--k')
plot(x, y*BFI3_m7_p(1)+BFI3_m7_p(2),'k'), hold off
ylim([0 1]), xlim([0 1])
xlabel('Local BFI3','FontSize',16)
ylabel('Station BFI3','FontSize',16)
title('Station BFI3 vs. Local BFI3','FontSize', 22)

%% Plot Residuals BFI calc vs BFI map (catchment <= 10,000)

figure(2)
subplot(1,2,1)
plot(BFI2t_map(BFI2_area <= 10000), ...
    (-1).*(BFI2t_map(BFI2_area<=10000).*BFI2_m2_p(1)+BFI2_m2_p(2))+BFI2t_calc(BFI2_area <=
10000), ...
    'r+','MarkerSize',3), hold on
plot(BFI2t_map(BFI2_area <= 5000), ...
    (-1).*(BFI2t_map(BFI2_area<=5000).*BFI2_m2_p(1)+BFI2_m2_p(2))+BFI2t_calc(BFI2_area <= 5000),
...
    'b+','MarkerSize',3)
plot([0 1],[0 0],'k')
xlabel('Downscaled BFI2','FontSize',16)
ylabel('Residuals','FontSize',16)
title('Residuals of Station BFI2 vs. Downscaled BFI2','FontSize', 17)
legend('Catchment Area >= 10,000 km^2','Catchment Area >= 5,000 km^2','','Location','southeast')

subplot(1,2,2)
plot(BFI3t_map(BFI3_area <= 10000), ...
```

```
    (-1).*BFI3t_map(BFI3_area<=10000).*BFI3_m2_p(1)+BFI3_m2_p(2)+BFI3t_calc(BFI3_area <= 10000),
...
    'r+','MarkerSize',3), hold on
plot(BFI3t_map(BFI3_area <= 5000), ...
    (-1).*BFI3t_map(BFI3_area<=5000).*BFI3_m2_p(1)+BFI3_m2_p(2)+BFI3t_calc(BFI3_area <= 5000),
...
    'b+','MarkerSize',3)
plot([0 1],[0 0],'k')
xlabel('Downscaled BFI3','FontSize',16)
ylabel('Residuals','FontSize',16)
title('Residuals of Station BFI3 vs. Downscaled BFI3','FontSize', 17)

%% BFI vs Catchment Area

% observed BFI2 vs catchment area
figure(3)
subplot(2,2,1)
plot(log10(BFI2_area),BFI2_calc,'b+','MarkerSize',3), hold on
plot([0 7],[0.75 0.75],'--k'), hold off
%title('BFI2 Observed vs. Log of Catchment Area','FontSize',16)
xlabel('Log of Catchment Area (km^2)','FontSize',16)
ylabel('Station BFI2','FontSize',16)
title('BFI2','Fontsize',20)

% observed BFI3 vs catchment area
subplot(2,2,2)
plot(log10(BFI3_area),BFI3_calc,'b+','MarkerSize',3), hold on
plot([0 7],[0.85 0.85],'--k'), hold off
%title('BFI3 Observed vs. Log of Catchment Area','FontSize',16)
xlabel('Log of Catchment Area (km^2)','FontSize',16)
ylabel('Station BFI3','FontSize',16)
title('BFI3','Fontsize',20)

% estimated BFI2 vs catchment area
subplot(2,2,3)
plot(log10(BFI2_area),BFI2_map,'b+','MarkerSize',3), hold on
plot([0 7],[0.75 0.75],'--k'), hold off
ylim([0 1])
%title('BFI2 Estimated vs. Log of Catchment Area','FontSize',16)
xlabel('Log of Catchment Area (km^2)','FontSize',16)
ylabel('Downscaled BFI2','FontSize',16)

% estimated BFI2 vs catchment area
subplot(2,2,4)
plot(log10(BFI3_area),BFI3_map,'b+','MarkerSize',3), hold on
plot([0 7],[0.85 0.85],'--k'), hold off
%title('BFI3 Estimated vs. Log of Catchment Area','FontSize',16)
xlabel('Log of Catchment Area (km^2)','FontSize',16)
ylabel('Downscaled BFI3','FontSize',16)

%% Data Histograms

text_size = 10;

% catchment size (catchments <= 10000 km^2)
figure(4)
subplot(4,1,1)
h = histogram(log10(BFI3_area(BFI3_area <= 10000)),'FaceColor','w');
h.BinWidth = 0.5;
title('Catchment Area < 10,000 km^2','FontSize',12)
ylabel('Num. of Catchments','FontSize',text_size)
xlabel('Log of Catchment Area (km^2)','FontSize',text_size)
```

```
ylim([0 650])

% record length (catchments <= 10000)
subplot(4,1,2)
h = histogram(BFI2_yrs(BFI2_area <= 10000),'FaceColor','w');
h.BinWidth = 10;
% title('','FontSize',16)
ylabel('Num. of Catchments','FontSize',text_size)
xlabel('Record Length (yrs)','FontSize',text_size)
xlim([10 150])
ylim([0 650])

% catchment size (all catchments)
subplot(4,1,3)
h = histogram(log10(BFI3_area),'FaceColor','#ADD8E6');
h.BinWidth = 0.5;
title('All Catchments','FontSize',12)
ylabel('Num. of Catchments','FontSize',text_size)
xlabel('Log of Catchment Area (km^2)','FontSize',text_size)
ylim([0 650])

% record length (all catchments)
subplot(4,1,4)
h = histogram(BFI2_yrs,'FaceColor','#ADD8E6');
h.BinWidth = 10;
% title('','FontSize',16)
ylabel('Num. of Catchments','FontSize',text_size)
xlabel('Record Length (yrs)','FontSize',text_size)
xlim([10 150])
ylim([0 650])
```